THE STUDY OF EXCITED OXYGEN MOLECULE GAS SPECIES PRODUCTION AND QUENCHING ON THERMAL PROTECTION SYSTEM MATERIALS

by

Paul C. Nordine,
Gordon T. Fujimoto,
and
Frank T. Greene

FINAL REPORT

June 24, 1986

NASA Contract No. NAS9-17261
MRI Project No. 8310-S

For

National Aeronautics and Space Administration
Houston, Texas 77058

Attn: Dr. Carl D. Scott/EC35
Mr. Mark A. Lucas/BE2

PREFACE

This report describes work to study the production of excited molecules by heterogeneous atom recombination on space vehicle thermal protection surfaces. Technical questions should be addressed to the authors. Drs. Nordine and Greene were co-principal investigators for the research. Dr. Fujimoto carried out the laboratory experiments. The sections of this report on field ionization detection of excited oxygen molecules are based on work by Professor Bret Halpern of Yale University who carried out the field ionization experiments.

The telephone number of Midwest Research Institute is (816) 753-7600.

Approved for:

MIDWEST RESEARCH INSTITUTE

W. D. Glauz, Director
Engineering and Materials
Sciences Department

June 24, 1986

TABLE OF CONTENTS

TABLE OF CONTENTS (Continued)

List of Figures

TABLE OF CONTENTS (Concluded)

List of Tables

ABSTRACT

The detection of excited oxygen molecules and ozone molecules formed by surface-catalyzed oxygen atom recombination and reaction was investigated by laser-induced fluorescence (LIF), molecular beam mass spectrometric (MBMS), and field ionization (FI) techniques. The experiments used partially dissociated oxygen flows from a microwave discharge at pressures in the range 60 to 400 Pa (0.5 to 3 torr) or from an inductively coupled RF discharge at atmospheric pressure. The catalyst materials investigated were nickel and the reaction-cured glass (RCG) coating used for Space Shuttle reusable surface insulation (RSI) titles.

Nonradiative loss processes for the laser-excited states make LIF detection of O_2 difficult such that formation of excited oxygen molecules could not be detected in the flow from the microwave discharge or in the gaseous products of atom loss on nickel or RSI. LIF detection of vibrationally excited (v=4,5,6) states of O_2 molecules was achieved in the flow from an atmospheric pressure RF discharge.

MBMS experiments showed that ozone was a product of heterogeneous O-atom loss on nickel and RSI surfaces at low temperatures (300K) and that ozone is lost on these materials at elevated temperatures. This can occur by reactions of adsorbed O-atoms only if the O-atom adsorption energies on the catalysts are less than 0.43 of the O-atom recombination energy. The formation of ozone is thus consistent with the small O-atom recombination energy accommodation coefficients that have been demonstrated for nickel and inferred for RSI, which also require low values for the O-atom adsorption energies.

Field ionization (FI) was separately investigated as a method by which excited oxygen molecules may be conveniently detected. Partial O_2 dissociation decreases the current produced by field ionization of the gas. This was attributed to a greater effect of O-atoms (whose ionization energy exceeds that of O_2) than of excited O_2 molecules formed in the microwave

discharge. Further work would be needed to establish the possibility of FI detection of excited O_2 molecules formed on TPS materials at high temperatures.

MBMS study of heterogeneous ozone formation provides a promising approach to further investigate the kinetics and energetics of O-atom reaction at TPS surfaces. Ozone is an easily detected product species whose formation is possible only when catalyzed O-atom loss delivers less than the full O-atom recombination energy to the catalyst surface. Similarily, MBMS study of heterogeneous nitrous oxide (N_2O) formation is needed to establish product species and to investigate the energetics of surface-catalyzed O-atom reactions of partially dissociated air.

I. INTRODUCTION

Upon entry into the atmosphere, the surfaces of a space vehicle are heated by the hot air produced in the bow shock in front of the vehicle. If peak deceleration occurs at a high altitude, where the ambient pressure is small, local thermochemical equilibrium is not achieved in the shock or in the thermal boundary layer between the shock and the vehicle surface. Energy transfer to the vehicle surface is then governed by the intrinsic kinetics of chemical and energy transfer processes.

Heterogeneous oxygen atom recombination is one of the more important processes by which re-entrant space vehicles are heated. The kinetics of atom recombination on space shuttle thermal protection system (TPS) materials have been investigated in two ways.[1,2] Atom recombination probabilities (γ) have been determined from measurements of the overall atom loss as dissociated oxygen and nitrogen were passed through a duct reactor whose walls were made from the TPS materials.[1] Large values of γ were obtained. But TPS heating rates in dissociated air that are characteristic of poor recombination catalysts have also been measured[2,3] in arc jet experiments. These two experiments suggest that TPS materials are good atom recombination catalysts that may produce highly excited product molecules that carry off most of the recombination energy.

Low values of the recombination energy accommodation coefficient, β, for recombining oxygen atoms have been demonstrated for a variety of materials by Melin and Madix.[13] They found, for example, that $\gamma = 0.017$ and $\beta = 0.16$ for O-atom recombination on nickel at room temperature. Thus, 90% of the energy released by O-atom recombination on nickel remains as internal energy of the product molecules and is not delivered to the nickel catalyst.

Studies of nonequilibrium effects on heat transfer rates during Space Shuttle entry of the atmosphere have been discussed by Scott.[4] Especially important are measurements of heating rates for highly catalytic TPS

tiles.[5,6] In these experiments, high temperature reusable surface insulation (RSI) tiles were coated with a highly catalytic material (C742, an iron-cobalt-chromia spinel) at several locations on the Space Shuttle surface. Elsewhere, the normal reaction-cured glass (RCG) coating was used. The C742-coated tiles displayed larger heating rates during space shuttle entry of the atmosphere to confirm that the RCG is indeed a poor catalyst and that nonequilibrium effects significantly reduce the surface temperatures that occur. These experiments were carried out under conditions that the O-atom and N-atom mass fractions were both approximately 0.2 at the edge of the thermal boundary layer.

The initial goals of this project were to directly detect and study the excited molecules produced by atom recombination on TPS materials and other materials, and to study the processes by which these molecules are quenched. Since the dissociation energy of O_2 is approximately half that of N_2, O-atoms achieve significant concentrations over a greater range of space vehicle re-entry conditions than do N-atoms. The emphasis of this work was accordingly on the detection and study of excited O_2 molecules.

The catalyst materials investigated were nickel and the reaction-cured glass coating of Space Shuttle tiles. The product molecules and excited states of product molecules formed by heterogeneous O-atom loss on these materials were investigated by laser-induced fluorescence (LIF) and molecular beam mass spectrometry. Partially dissociated oxygen was formed in these flow system experiments by using either a microwave discharge at pressures in the range 60 to 400 Pa (0.5 to 3 torr) or an inductively coupled RF discharge at atmospheric pressure. Attempts to operate the RF discharge at reduced pressures were not successful due to excessive heating of quartz or alumina tubes used to contain the discharge.

Excited oxygen molecules were not produced in sufficient quantities for LIF detection with the microwave discharge technique or by atom loss on nickel or RSI. The high detection limit for excited O_2 in these experiments resulted from nonradiative loss processes for the laser-excited states.

The concentration of vibrationally excited (v = 4,5,6) states of O_2 molecules was sufficient in the experiments with an RF discharge for LIF detection via laser excitation to the O_2 B-state. The pressure was too large in these experiments for observation of heterogeneous atom loss affects and the LIF spectrum was unchanged when RSI was located near the point at which LIF was observed.

During this work, it was recognized that the energy balances for O-atom loss on some materials[13] allow production of O_3 (ozone) from heterogeneous $O + O_2$ reaction in partially dissociated oxygen and of N_2O (nitrous oxide) from heterogeneous $O + N_2$ reaction in partially dissociated air. The energy released by these reactions is less than that of O-atom recombination. Formation of ozone and/or nitrous oxide could thus contribute to the small energy accommodation coefficients that have been observed for O-atom loss on TPS and other materials. Molecular beam mass spectrometry (MBMS) was therefore used to investigate ozone formation during O-atom loss on RSI and nickel and to independently investigate the rates of O-atom loss on these materials. The partially dissociated oxygen flows were formed by the microwave discharge techniques. The results showed that small quantities of ozone were formed on nickel and RSI at room temperature and that ozone was lost on the catalyst surfaces at elevated temperature. However, atom loss probabilities were sufficient to produce diffusion limited O-atom loss rates at the catalyst surfaces. This made the results insensitive to the gas-surface reaction rates to produce O_2 by O-atom recombination and O_3 by O-atom reaction with O_2.

Finally, field ionization (FI) was separately investigated as a method by which excited oxygen molecules could be conveniently detected. Excited molecule detection was demonstrated in microwave discharge flow system experiments. This technique has some promise for basic research on atom recombination kinetics. Much further work would be needed to use it for detecting excited molecules formed on TPS materials at high temperature.

The experimental investigation of specific excited molecules formed by oxygen-atom loss has proven to be very difficult by the methods employed in this work. However, a number of experiments that go beyond the scope of this work are feasible that would help to understand the kinetics of TPS heating during space vehicle reentry. Experiments are suggested that involve MBMS detection techniques in flow systems operated at the gas pressures and catalyst temperatures encountered during space vehicle reentry. Kinetic data on heterogeneous O-atom loss as well as O_2, O_3, and N_2O production may thus be obtained. Further development of the FI technique is suggested to provide basic results on the product species formed by atom recombination on model materials.

II. PRODUCTS OF HETEROGENEOUS O-ATOM LOSS

Heterogeneous loss of atomic oxygen may occur by reaction with the surface, by surface-catalyzed recombination of O-atoms to form O_2, and by surface-catalyzed reaction of O-atoms with other gaseous species to form gaseous products other than O_2. Since reactions of O-atoms are usually quite exothermic, excited oxygen and other molecular product species are possible.

Rates of atom recombination and energy accommodation are conventionally reported in terms of the dimensionless recombination probability, γ, and the recombination energy accommodation coefficient, β. γ is the probability that an atom which strikes the surface will be emitted as part of an O_2 molecule. β is the fraction of the molecular dissociation energy that is absorbed by the surface when heterogeneous atom recombination occurs. These parameters can be calculated from measurements of atom concentration at the entrance and exit of a reactor in which recombination occurs, and

from energy balance measurements on the surface. Melin and Madix[13] report the following values of γ and β for O-atom recombination on several metals and pyrex at ca. 300K (Table 1):

TABLE 1

O-ATOM RECOMBINATION AND ENERGY ACCOMMODATION COEFFICIENTS[13]

Material	Probability, γ	Energy Accommodation Coefficient, β
Ag	0.24	0.95
Au	0.008	0.17
Co	0.075	0.67
Cu	0.015	0.30
Fe	0.010	0.07
Ni	0.017	0.16
Pt	0.014	0.10
W	0.013	0.09
Pyrex	0.00013	-

A. Ozone and Nitrous Oxide

The assumption that surface-catalyzed loss of O-atoms occurs via O_2 production was made in the calculation of values for β given in Table 1. But in many cases, ozone (O_3) was an energetically possible product of heterogeneous reaction in the partially dissociated oxygen used in the experiments from which these values were derived.

Table 2 presents data about the energetics of O-atom reactions to produce O_2, O_3, and N_2O. The maximum apparent value of the recombination energy accommodation coefficient, $\beta_{max,app}$, occurs if the entire energy of the associated reaction is absorbed at the catalyst surface. These apparent values of β represent the maximum value that may be observed if the given reaction is the principle mechanism of O-atom loss.

TABLE 2

ENERGETICS OF O-ATOM LOSS PROCESSES

Reaction	ΔH°_{300}, kcal/mol	$\beta_{max,app}$
$O + O = O_2$	-119.1	1.00
$O + O_2 = O_3$	-25.5	0.43
$O + N_2 = N_2O$	-40.0	0.67

Thus, if the reported value of β in $O + O_2$ mixtures is less than 0.43, O_2 or O_3 may be the primary product of O-atom reaction. If β is reported to be less than 0.67 in an $O + N_2$ mixture, O_2, or N_2O may be the primary product of O-atom loss. It can thus be seen from the data in Table 1 that ozone is an energetically possible product for O-atom recombination on Au, Cu, Fe, Ni, Pt, and W. Similarly, ozone and nitrous oxide are possible products of atom loss on space vehicle TPS materials.

B. Excited Oxygen Molecules

Potential energy curves given by Krupenie[8] for O_2 are reproduced in Figure 1. It may be seen that recombination of ground state (^3P) oxygen atoms can produce six different electronic states of O_2, for which properties are given in Table 3. The table includes properties for the $^5\Pi_g$ state that have been calculated by Saxon and Liu.[9] These are the states that may be produced by (^3P) O-atom recombination. Table 3 also includes properties for the well known B $^3\Sigma_u^-$ state of O_2.

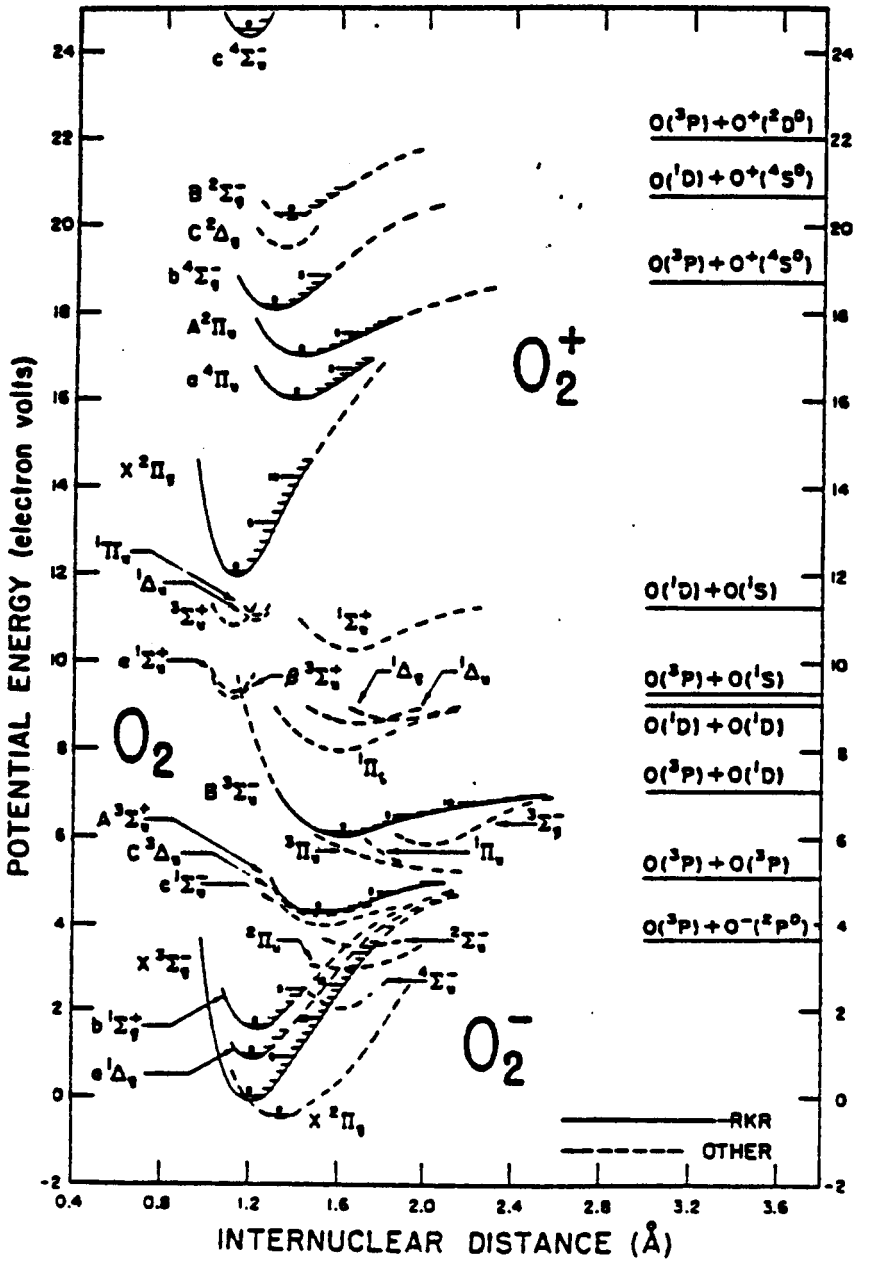

Figure 1 - Potential Energy Curves for O_2. From Krupenie.[8]

TABLE 3

PROPERTIES OF O_2 MOLECULES FORMED BY RECOMBINATION OF $O(^3P)$ ATOMS[8-10]

Electronic State	Internuclear Distance	Potential Energy (v=0)	Radiative Lifetime
$X\ ^3\Sigma_g^-$	0.1208 nm	0.000 ev	-
$a\ ^1\Delta_g$	0.1216	0.977	3880 s, a-X
$b\ ^1\Sigma_g^+$	0.1227	1.626	12 s, b-X
$c\ ^1\Sigma_u^-$	0.1517	4.049	25-50 s, c(v=0-10)-X
$C\ ^3\Delta_u$	0.15	4.254	10-100 s, C(v=6, Ω=2)-X 5-50 s, C(V=0-6, Ω=1)-a
$A\ ^3\Sigma_u^+$	0.1522	4.391	160-250 ms, A(v=0-6)-X
$^5\Pi_g$	0.20	4.88	-
2 $O(^3P)$ atoms		5.115	
$B\ ^3\Sigma_u^-$	0.1604	6.175	
$O_2^+\ X\ ^2\pi_g$	0.111	12.08	

Emission spectra have shown that microwave discharges can produce oxygen molecules in a variety of electronic and vibrational levels. Slanger[10] observed in the wake of a discharge emission from the b, c, C, and A states by using a spectrograph equipped with an image intensifier tube. Emission of the Schumman-Runge bands by the B state is well known,[8] as is the "dimole" emission[11,12] from the state:

$$2\ O_2(^1\Delta_g) = 2\ O_2(^3\Sigma_g^-) + h\upsilon \qquad (1)$$

Heterogeneous recombination of $O(^3P)$ atoms can also produce various electronically excited states of O_2. Harteck et al.,[14] report that O_2 $(A\ ^3\Sigma_u^+)$ is efficiently formed by O-atom recombination on a nickel surface. Kenner and Ogryzlo[17,18] have used this effect to obtain kinetic data on O_2 $(A\ ^3\Sigma_u^+)$ and O_2 $(c\ ^1\Sigma_u^-)$ molecules.

III. EXPERIMENTAL

In this work, discharge flow reactor techniques were used to produce oxygen atoms. Laser-induced fluorescence (LIF), molecular beam mass spectrometry (MBMS), and field ionization (FI) were the methods selected for detecting excited molecules and the products of heterogeneous O-atom reaction on nickel and RSI. The partially dissociated and excited flows of oxygen were formed by microwave discharges, atmospheric pressure RF discharges, or by flowing O_2 gas over an electrically heated filament.

A. Microwave Discharge Flow Reactor

The microwave discharge flow reactor is depicted in Figure 2, whose caption identifies the reactor components. A 2,450 MHz microwave discharge was operated typically at 60 w in the 10 mm ID discharge tube from which gases flowed into a 7.6 cm ID flow tube. The quartz discharge tube was periodically treated with phosphoric acid to decrease wall loss of

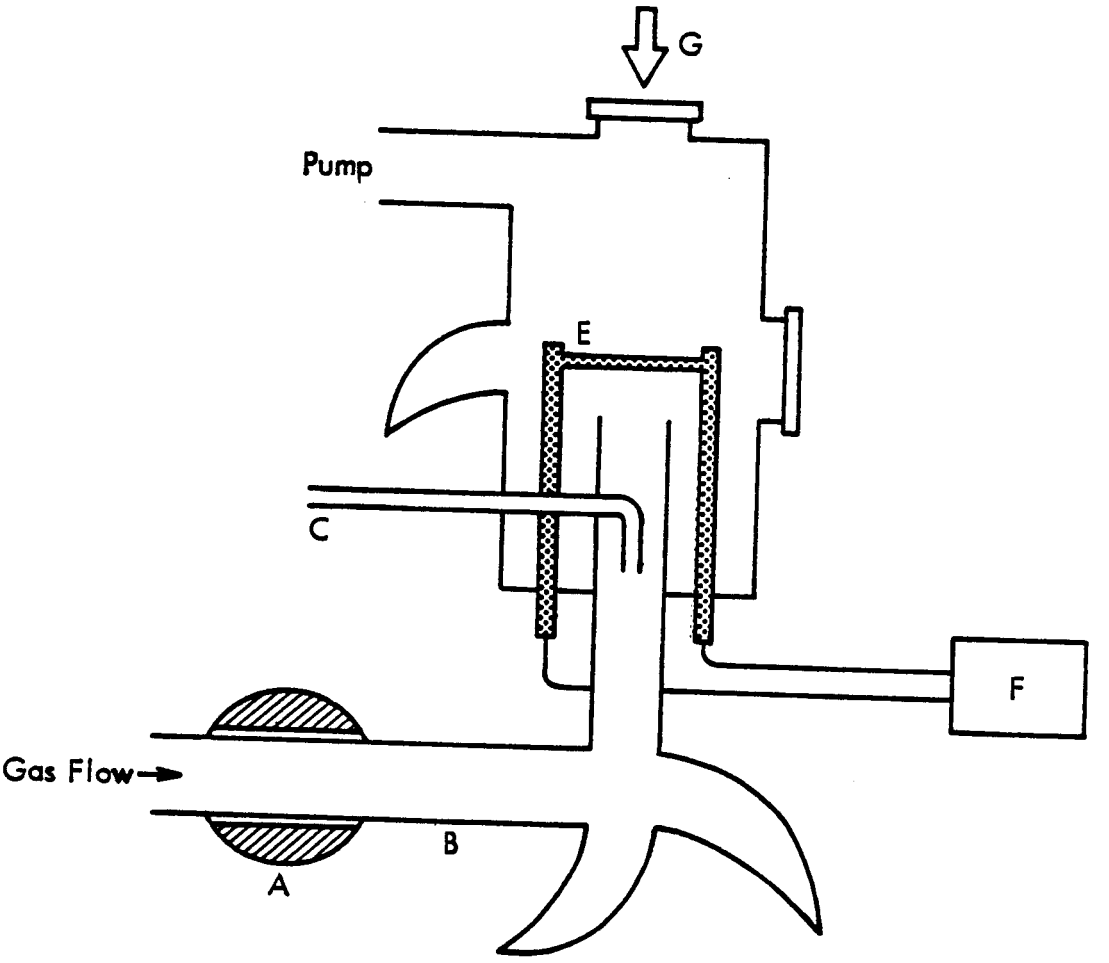

Figure 2 - Side View of Flow Reactor. A - 2,450 MHz, 60 w microwave discharge; B - quartz flow tube; C - titration gas inlet; E - atom recombination catalyst or heating element; F - power supply used for heating metal specimens; G - CW CO_2 laser beam for heating TPS materials.

atoms produced in the discharge and increase the atom concentration. Gas pressure in the flow tube was measured with an electronic manometer and typically maintained at 0.5 to 1.0 torr by a 27 cfm mechanical pump. A titration gas inlet allowed chemiluminescent titrations to measure atom concentrations via the O/NO_2 reaction and to measure N-atom concentrations via the N/NO reaction. Flow velocities at the discharge tube exhaust were typically 1,000 cm/s.

The recombination catalysts were in the form of thin wires or ribbons that could be electrically heated and were located about 2 cm from the exhaust of the discharge tube. Most of the experiments employed a nickel ribbon as the recombination catalyst, since nickel is known to have a small accommodation coefficient for the energy released by O-atom recombination.

For experiments with dissociated O_2 gas, the gas mixture passed through the discharge tube was typically 0.5 to 1.0 torr argon to which 0.05 to 0.20 torr oxygen was added. Oxygen-atom production in the discharge varied such that typical O-atom concentrations were 10^{14} to 10^{15} cm^{-3}, depending on time since the discharge tube was last treated with phosphoric acid. This range includes an approximate two-fold day-to-day variation in atom production that depended on time since the discharge tube was last exposed to the atmosphere. The O-atom concentrations measured by chemilumenscent titrations were checked by observing a large temperature increase in a silver wire recombination catalyst when the microwave discharge was turned on.

The percentage of O_2 molecules dissociated in the discharge was never more than 30%. To obtain O-atom flows that were substantially free of undissociated O_2, nitrogen gas was passed through the discharge and the resulting N-atoms titrated with NO according to the reaction:

$$NO + N = N_2 + O \qquad (2)$$

This allowed the possible quenching effects of ground state O_2 molecules to be reduced in experiments to detect excited O_2 molecules produced by O-atom recombination.

In a separate experiment, a thin Kanthal heating element was substituted for the recombination catalyst and electrically heated to about 1500K for laser induced fluorescence experiments on vibrationally excited O_2 molecules.

The setup for LIF experiments is illustrated in Figure 3, whose caption identifies the components. The Nd/YAG pumped dye laser system provided ca. 15 ns pulses of radiation within a 0.3 cm^{-1} bandwidth in the wavelength range 217 nm to at least 700 nm, which was focused to ca. 0.1 cm diameter beam that passed through the analysis retion. Fluorescence from excited molecules was collected by an F-5 suprasil quartz lens, passed through appropriate filters and/or a 1/4 m monochromator onto a Hamamatsu R212 or R166 photomultiplier tube. The output of the photomultiplier was measured with an EG&G PAR model 162/165 boxcar averager.

Radiative lifetimes, quenching rates, and rates of other nonradiative loss processes for the excited states of O_2 are not well enough understood to predict LIF detection limits for the excited states of O_2 of interest in this work. Therefore, a number of exploratory experiments to detect these molecules were performed. The particular transitions pumped by the laser and wavelengths at which fluorescence was monitored are given in the results. These experiments were performed in the wake of a nickel ribbon atom recombination catalyst or a Kanthal ribbon heating element that was electrically heated to 1500K as measured with an optical pyrometer and in the direct output of the microwave discharge.

The apparatus was tested by measuring LIF from NO and OH molecules. The NO was added to the gas flow in known amounts and the OH molecules were produced by passing an $Ar/O_2/H_2$ mixture through the discharge or over a

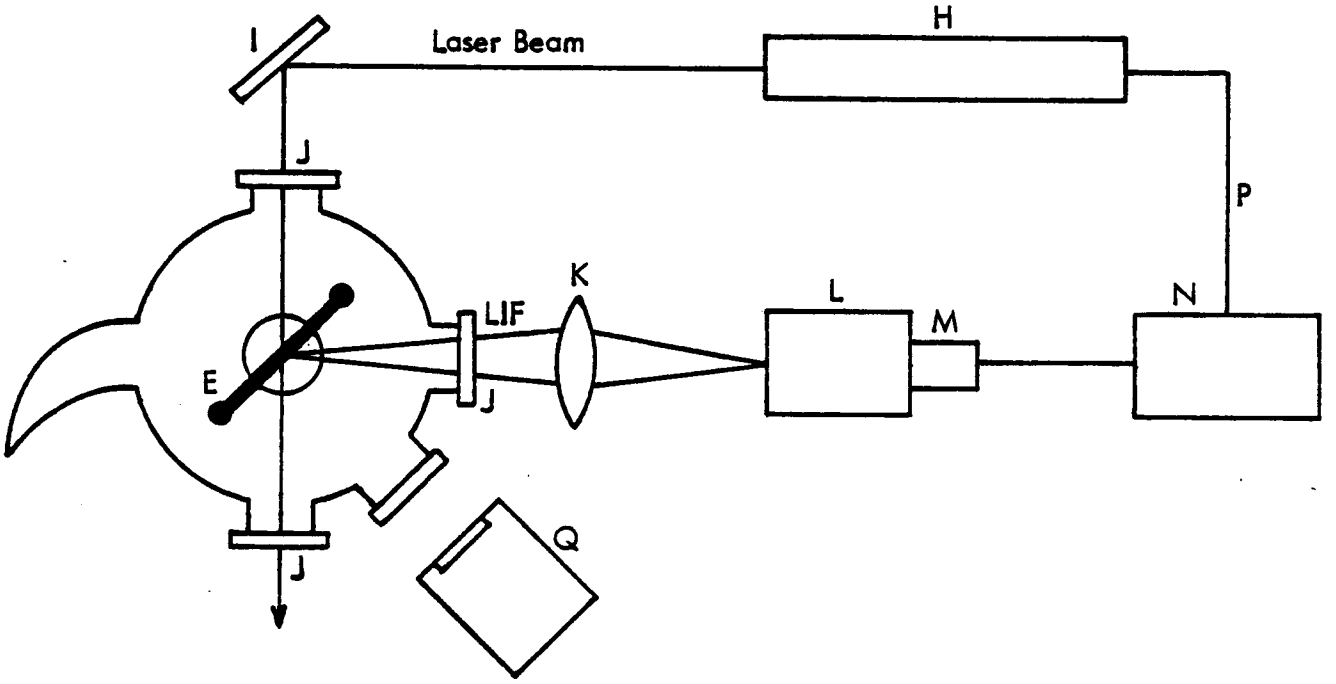

Figure 3 - Top View of Flow Reactor and Laser-Induced Fluorescence Apparatus. E - atom recombination catalyst or heating element; H - Nd/YAG pumped dye laser system; I - laser beam steering device; J - Suprasil quartz windows; K - lens used to collect laser induced fluorescence; L - interference filter or 1/4 meter monochromator; M - photomultiplier; N - boxcar averager; P - laser trigger; Q - optical pyrometer.

platinum filament heated to about 1300K. In the NO experiments the A(v=0) ← X(v=0) transition was laser pumped at 225 nm and LIF detected on the A(v=0) → X(v=0 to 8) transitions. The OH radicals were detected by laser pumping of the A(v=1) ← X(v=0) transition at 282 nm and observing fluorescence from the A(v=1) → X(v=1) transition.

B. Field Ionization System

The apparatus for field ionization detection of excited molecules is illustrated in Figure 4. There were two basic parts to this sytem. One was a fast flow line for atom generation and the other was the field ionization tube, with its own vacuum system. The atom flow path is marked with arrows in the figure. The pressure in the atom flow line was about 1 torr and the pressure in the ionization tube was about 10^{-3} torr. Gas flowed into the field ion tube via a small orifice in the glass atom line of about 0.005 cm diameter.

The field ionization tip radius was approximately 10^{-4} cm. When operated at a potential of a few thousand volts, the electrical field was sufficient that molecules and atoms in the vicinity of the tip were ionized at a rate that depended on the ionization energy. Incident excited O_2 molecules and O-atoms that recombined on the tip to form excited O_2 molecules were detected because they produced ion currents at tip voltages lower than the voltage required to ionize ground state oxygen molecules.

C. RF Discharge Flow Reactor

Figure 5 is a side view of the inductively coupled RF discharge flow reactor. An Ar/O_2 plasma was driven by a 5 kW, 3 MHz RF power supply. TPS or other materials were placed in the flow to study the influence of heterogeneous atom recombination and excited molecule quenching on the vibrationally excited molecules that were present. An optical pyrometer was used to measure specimen temperature.

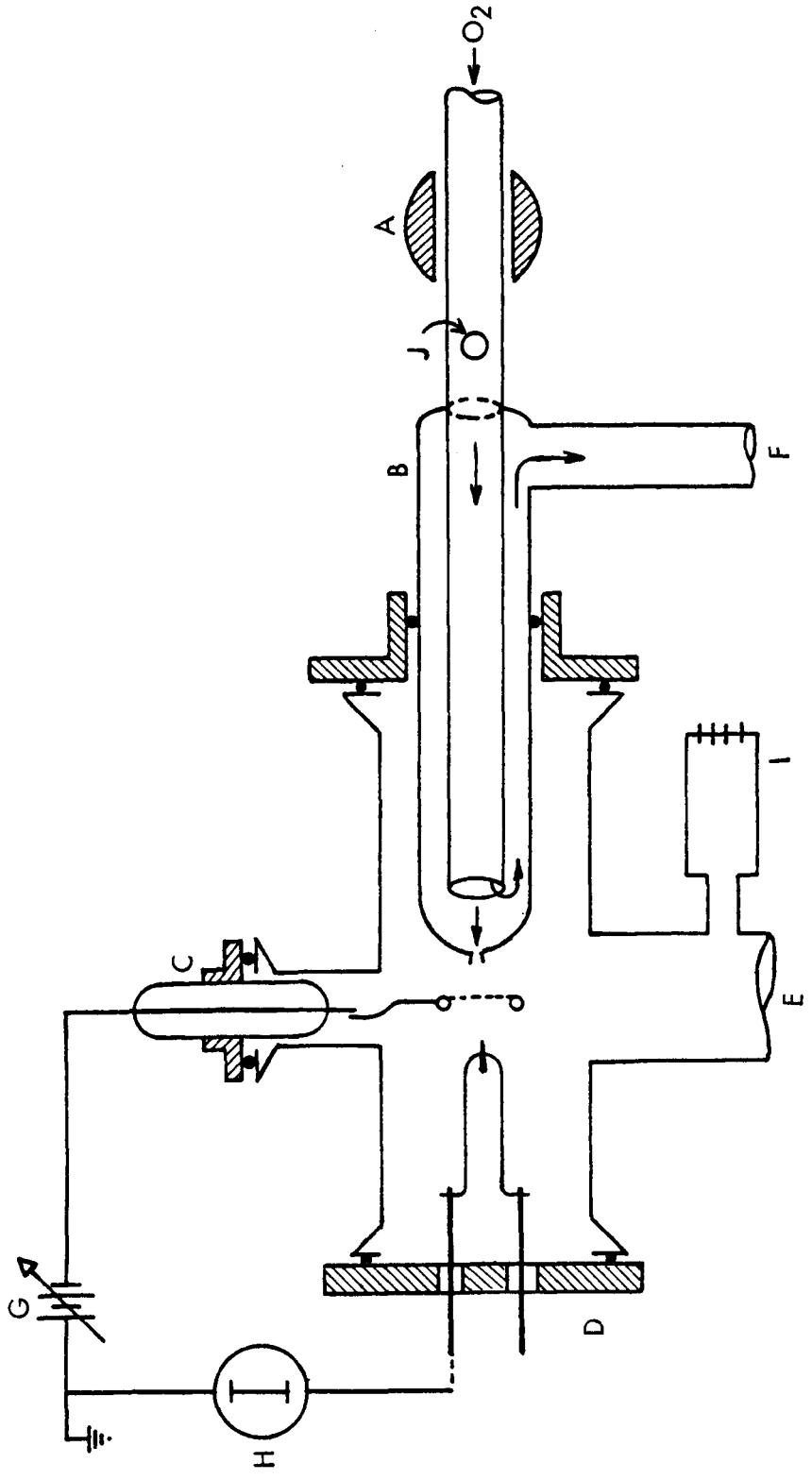

Figure 4 - Apparatus for Field Ion Detection of Excited Molecules. A - 2,450 MHz microwave discharge; B - glass flow line for atom generation: orifice diameter ca. 0.005 cm; C - high voltage lead; D - "tip" assembly: brass flange with feed throughs, wire loop, and field emitter; E - to oil diffusion pump and mechanical pump No. 1; F - to mechanical pump No. 2; G - 10 KV supply; H - Keithley electrometer; I - Schulz-Phelps pressure gauge; J - side arm for inserting nickel wire coil into the flow.

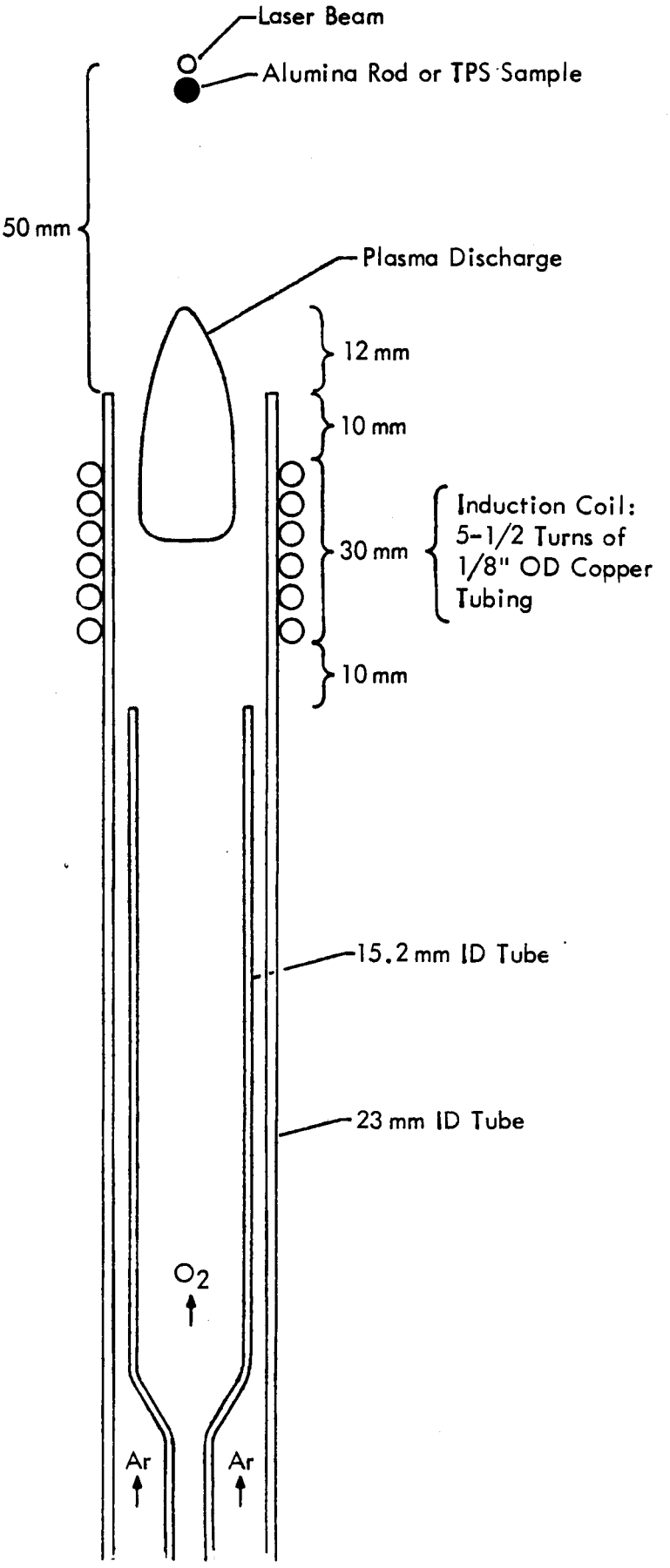

Figure 5 - Side View of the Plasma Discharge Apparatus

The figure illustrates an experiment in which a 0.16 cm diameter alumina rod was placed in the flow, where it was heated to approximately 1980K. LIF measurements were then obtained in the wake of the alumina rod. LIF measurements were also obtained from the same location without the catalyst material and with an RSI specimen placed near the location where LIF was produced.

RF coil and flow tube design, ambient pressure, gas flow rates, and RF power were varied to discover conditions under which stable operation was possible. The initial experiments used a closed quartz tube that was operated at reduced pressures. However, it was then possible to operate the plasma without melting the quartz tube only at minimum power in argon.

Another difficulty in operation of the plasma involved an afterglow produced when the plasma contacted the quartz flow tube wall. The afterglow intensity was sufficient to prevent LIF detection of excited O_2 molecules.

Stable, afterglow-free plasma operating conditions were developed at atmospheric pressure, where the flow tubde did not immediately collapse when heated to the softening point by the discharge. Careful centering of the inner flow tube that carried oxygen gas in the outer tube that carried argon gas was necessary. The gap between the visible discharge and the quartz tube increased with the length of the expanded section of the oxygen flow tube. At least 10 cm was appropriate for this length. The afterglow could not be avoided if the flow tube was accidentally heated to the softening point so that it sagged or became slightly distorted. Best operation at atmospheric pressure was obtained when the coil was tightly wound on the quartz flow tube. For operation at reduced pressure it was best to leave a gap between the coil and quartz tube.

The optical system is illustrated in Figure 6. The laser beam passed through the wake of the discharge at a distance (as illustrated in Figure 5) of about 5 cm above the center of the discharge. The plasma was a very intense light source which required careful design for stray light

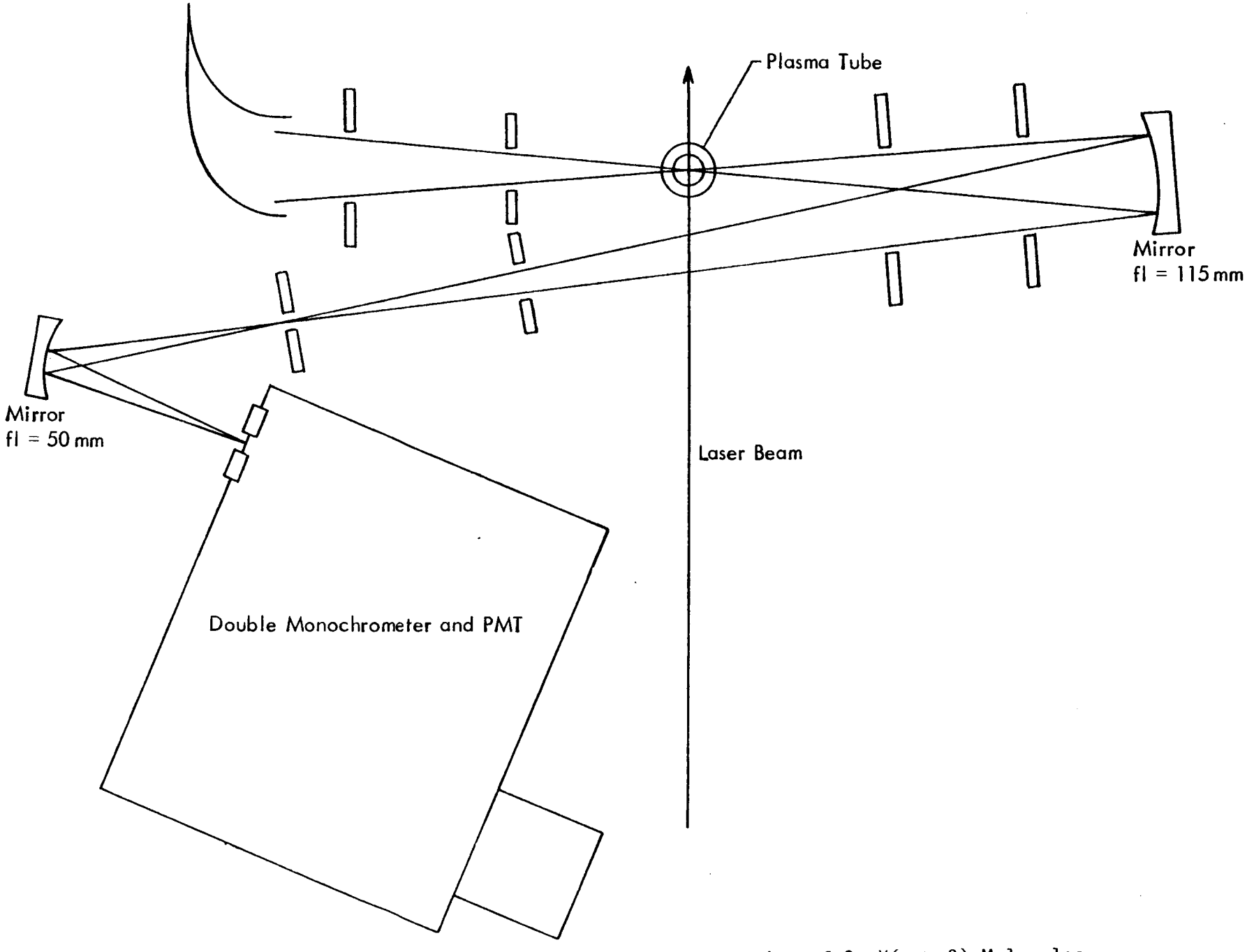

Figure 6 - Optical Design for LIF Detection of O_2 X(v > 3) Molecules Produced by the RF Plasma

rejection, even at the ultraviolet wavelengths used for LIF experiments. The light trap and shields with apertures illustrated in the figure were adequate for detecting LIF at wavelengths below 350 nm.

D. Molecular Beam Mass Spectrometric Apparatus

In the molecular beam sampling technique, the gas to be sampled is drawn through a small orifice in the sampling probe and expanded to collisionless flow in a free-jet. This free-jet is then collimated into a molecular beam which is introduced into the ion source of the mass spectrometer. Because the free-jet expansion produces an extremely rapid drop in temperature and pressure, thereby quenching the sampled species, and because the sampled gas does not contact any surfaces during sampling and mass spectrometric analysis, MBMS can be used to study unstable species ranging from free radicals to high temperature oxides. Also, this technique is capable of high analytical precision since the beam formation process is highly reproducible.

The MBMS system used on this program is shown in Figure 7. The reaction gas was sampled through a 0.046 cm diameter orifice in the tip of a 90-degree spun copper cone which was maintained at ambient temperature. The molecular beam was detected by a modified EAI quadrupole mass spectrometer directed in the "cross-beam" mode as shown. The molecular beam was chopped by a rotating sector, and phase sensitive detection employed to discriminate against background gas in the mass spectrometric stage and to improve the signal-to-noise ratio. All measurements were made using an ionizing energy of 50 ev.

The flow reactor used for the MBMS experiments is shown in Figure 8. The experiments were carried out with the RSI specimen first located at a distance about 2 cm from the flow axis. The gas flow was stabilized, the RSI specimen was heated to the temperature of interest and the O^+ and O_2^+ ion intensities measured with the mass spectrometer. This established the contribution of dissociative O_2 ionization to the O^+ ion intensity. The

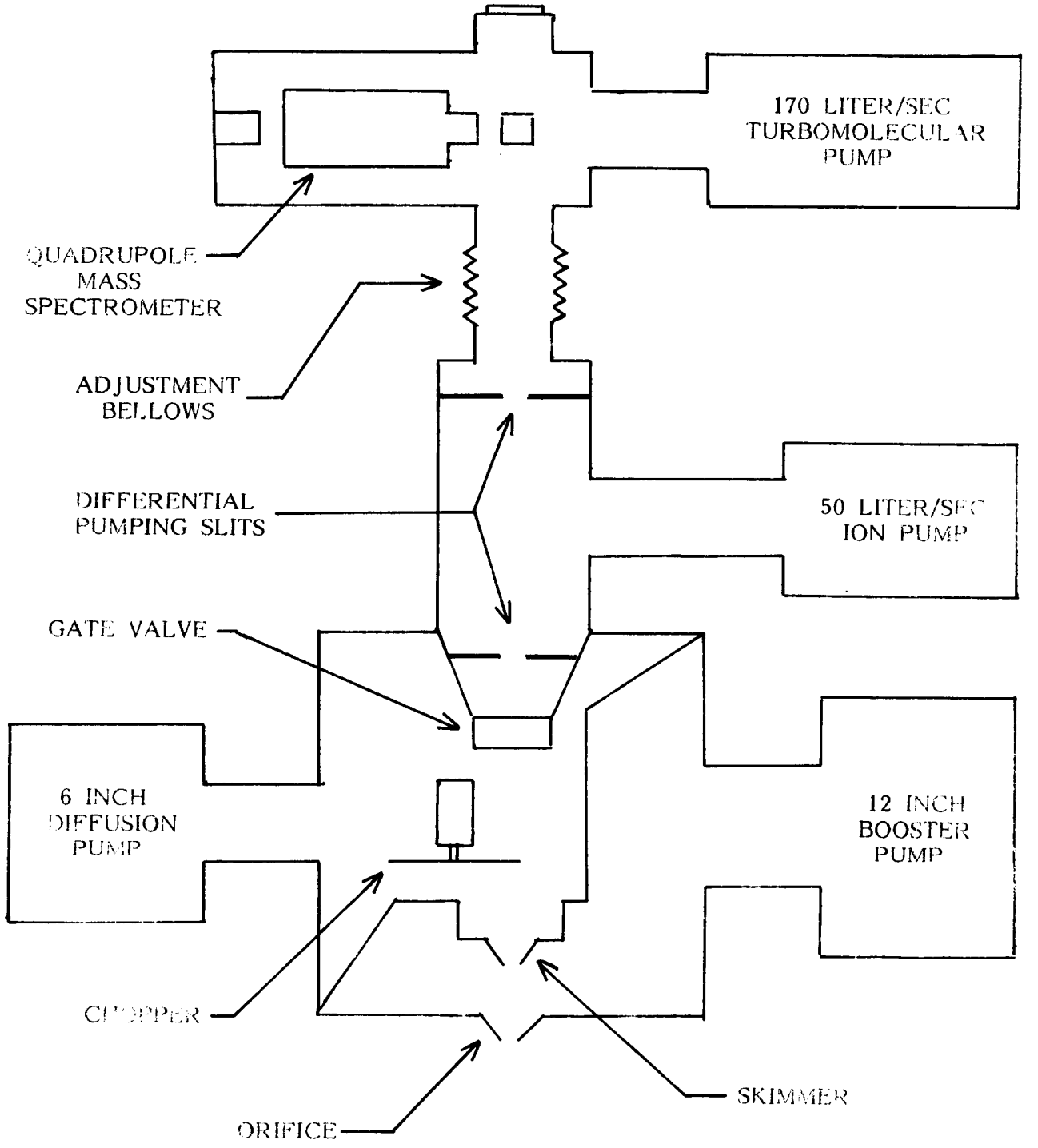

Figure 7 - Molecular Beam Mass Spectrometric (MBMS) System

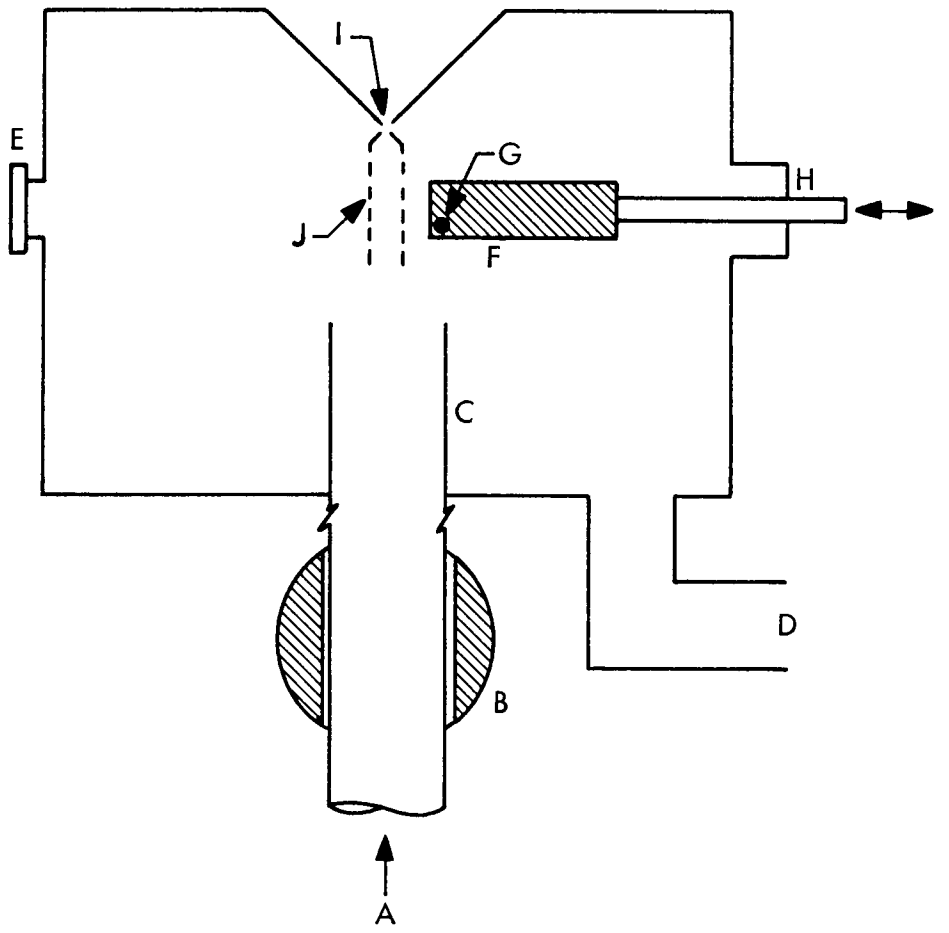

Figure 8 - Flow Reactor for MBMS Experiments. A - Argon + oxygen gas flow; B - 2,450 MHz, 60 w microwave discharge; C - 1 cm ID quartz flow tube, exit located 17 mm from the MBMS orifice; D - to vacuum pump; E - pyrex window for optical pyrometry; F - RSI specimen, edge height approximately 0.5 cm; G - Kanthal wire heating element; H - mechanical and electrical feedthroughs for positioning and heating the RSI specimen; I - 0.046 cm diameter MBMS sampling orifice; J - approximately 0.10 cm diameter flow sampled by the MBMS orifice that was assumed for design calculations and discussion of results.

microwave discharge was then turned on and stabilized, and the O^+, O_2^+, and O_3^+ ion intensities measured as the RSI specimen was moved into the gas flow from the discharge tube.

The RSI specimens were semitransparent at the wavelength, 0.66 μm, at which the optical pyrometer operated. The apparent temperature of the Kanthal wire heating element was measured by viewing it with the pyrometer through the RSI surface during the MBMS experiments. The RSI surface temperature was determined with a thermocouple in separate calibrations at the same apparent Kanthal wire temperature.

MBMS experiments were carried out with RSI specimens at temperatures up to 600°C. Experiments with nickel catalysts used nickel foil closely wrapped over an RSI sample. Direct electrical resistance heating of the nickel foil was used for experiments at elevated temperatures. The bottom edge of the specimens was rounded for RSI and square for nickel.

Flow reactor pressure limits for the MBMS experiments: The MBMS experiments were designed such that the catalyst could be placed sufficiently close to the flow sampled by the MBMS orifice that surface-catalyzed atom loss could be observed. Also, flow distances were minimized to avoid diffusive mixing of ambient gas with that flowing from the discharge to the MBMS orifice. Two criteria involving gas diffusion and flow times are discussed below that were thus used to choose flow reactor operating conditions. These criteria involve flow times fixed by the dimensions and pumping rates of the system and diffusion times that depended on the dimensions and reactor pressure. The fluid flow model used for these analyses assumed a cylindrical flow field within which the mass flow from the discharge equaled that through the MBMS orifice, as is illustrated in Figure 8.

The average flow velocity at the exit of the discharge tube was $u = 1{,}970$ cm/sec as determined by the measured gas flow rate at a reactor pressure of 4,000 Pa (3.0 torr) and the discharge tube diameter. The flow velocity at the center of the discharge tube was twice this value due to laminar flow from the discharge tube. The distance from the discharge tube

exit to the MBMS orifice was 1.7 cm so that the discharge tube to MBMS flow time was t = 0.43 ms. The time required for gas flow past the 0.5 cm high RSI specimen edge was t' = 0.13 ms.

The volumetric sampling rate of the MBMS system was calculated assuming choked flow at the MBMS orifice. This equaled the flow of gas delivered by a 0.10-cm diameter cylindrical section of the flow from the discharge tube as is indicated in Figure 8. This diameter and the discharge tube diameter set the diffusion distances used to choose reactor operating pressures.

The upper limit on reactor pressure was obtained by requiring that the distance, x', that molecules would diffuse in the time t' for gas flow past the RSI specimen, exceeded the sampled flow diameter, i.e., that

$$x' = (Dt')^{0.5} > 0.10 \text{ cm} \qquad (3)$$

This criterion ensured that most of the O-atoms in the gas sampled by the MBMS system would interact with the recombination catalyst when the catalyst is located next to the sampled gas flow. With a diffusion coefficient for O-atoms in argon approximately D = 200/P(torr) cm^2/sec, at 300K, we obtained P < 2.6 torr from this criterion.

The lower limit on reactor pressure resulted from the requirement that ambient gas molecules not diffuse into the sampled flow in the time, t, for gas flow from the discharge tube to the MBMS orifice. The distance, x, that these contaminant molecules would have to diffuse is half the difference between the discharge tube and sampled gas flow diameters, i.e.,

$$x = (Dt)^{0.5} < 0.45 \text{ cm} \qquad (4)$$

From this requirement we obtained a lower limit on the reactor pressure, P > 0.5 torr.

The criteria given above are approximate. A more exact analysis would account for gas heating by the hot RSI sample, and pressure dependent reactor pumping speed. The main effect of gas heating would be to increase the diffusion coefficient for oxygen atoms in argon, which would lead to an increase of both of the pressure limits calculated above. It was concluded that reactor operation at a pressure of 3 torr would allow good sensitivity to atom loss at the RSI specimen and that little mixing between the sampled gas flow from the discharge tube and ambient gas molecules would occur at the RSI temperatures (up to 900K) achieved in the experiments.

IV. RESULTS

A. Laser-Induced Fluorescence Experiments

LIF was easily observed from NO molecules. The minimum detectable concentration of specific rovibronic states of NO molecules was about 2×10^9 cm^{-3}.

Nonradiative loss of the excited NO molecules produced by the laser may be neglected so that the intensity of LIF in the experiments with NO is given by:

$$I = n\ f\ V\ e \qquad (5)$$

where I is in photons detected per laser pulse, n is the concentration of molecules in the particular rovibronic state pumped by the laser, f is the fraction of these molecules that is excited by the laser pulse, and V is the volume (ca. 10^{-3} cm^3) from which LIF was collected with an efficiency, e. The value of e was approximately 5×10^{-6}, with an F-5 lens, 20% monochromator transmission, 10% quantum efficiency for the photomultiplier, and with about 10% of the emitted LIF within the detected bandwidth. The laser intensity was sufficient to saturate the NO $A \leftarrow X$ transition so that $f = 1/2$. Thus, we obtain a minimum detectable intensity approximately equal to 5 photons per laser pulse.

Table 4 lists the transitions used to attempt detection of electronically excited oxygen molecules in the products of O-atom recombination on nickel with the microwave discharge flow reactor system. The LIF intensity in these experiments was below the detection limits. Excited O_2 detection was also unsuccessful in the gases produced by the microwave discharge when the nickel catalyst was not used.

Table 5 lists the transitions used to attempt detection of vibrationally excited oxygen molecules in oxygen at 100 torr and T = 1500K in the vicinity of a hot Kanthal filament. The v=4,5 molecules were detected by laser excitation to the B state but not by excitation to the A state. The concentration of O_2 X(v=5) molecules was just sufficient for detection. The v=3 state was not detected because the B(v=0) ← X(v=3) transition was the only one available within the lower wavelength limit of the laser, and this transition is very weak compared to those used to detect v=4,5 molecules. An example of LIF spectrum taken of the X(v=4) level is presented in Figure 9.

Figures 10 and 11 present LIF spectra obtained via the B $\leftrightarrow$ X $^3\Sigma_g^-$ transitions with the RF discharge flow reactor. Peaks arising from laser excitation of different rotational levels of the v=4,5,6 vibrational levels of the O_2 ground state are identified in the figures. The intensities of v=6 lines are sufficient that it is likely that excitation of v=7 and v=8 molecules contribute some of the unidentified weak lines.

Spectra obtained with the RF discharge flow reactor displayed relative intensities for different vibrational levels that did not change when the alumina rod or RSI specimen was placed in the flow. It was concluded that the gas pressure in these experiments (one atmosphere) was too large for detection of molecules produced by heterogeneous atom recombination. Also, it appeared that heat transfer to these specimens did not produce a change in the gas temperature sufficient that a change in vibrational populations could be detected.

TABLE 4

TRANSITIONS USED IN LIF EXPERIMENTS ON ELECTRONICALLY EXCITED O_2

State to be Detected	Laser Excitation	Fluorescence
$a\ ^1\Delta_g$	A ← a (3,0) - 340 nm	A → X (3,4) - 321 nm
	A ← a (4,0) - 333 nm	A → X (4,4) - 314 nm
	A ← a (5,0) - 326 nm	A → X (5,3) - 294 nm
	A ← a (6,0) - 319 nm	A → X (6,2) - 277 nm
	A ← a (7,0) - 314 nm	A → X (7,2) - 273 nm
	A ← a (3-7,0)	A → X (0,8) - 431 nm (1)
	A ← a (3-7,0)	c → X (0,6) - 422 nm
	C ← a (4,0) - 343 nm	C → X (4,3) - 308 nm
	C ← a (5,0) - 336 nm	C → X (5,2) - 289 nm
	C ← a (6,0) - 330 nm	C → X (6,2) - 284 nm
	C ← a (7,0) - 324 nm	C → X (7,1) - 268 nm
	C ← a (8,0) - 318 nm	C → X (8,1) - 264 nm
	C ← a (9,0) - 313 nm	C → X (9,0) - 251 nm
	C ← a (4-9,0)	C → X (0,8) - 444 nm (1)
	c ← a (4-9,0)	c → X (0,6) - 422 nm (2)
	c ← a (5,0) - 353 nm	c → X (5,7) - 387 nm
	c ← a (6,0) - 345 nm	c → X (6,7) - 378 nm
	c ← a (7,0) - 339 nm	c → X (7,7) - 370 nm
	c ← a (8,0) - 333 nm	c → X (8,7) - 363 nm
	c ← a (9,0) - 327 nm	c → X (9,4) - 309 nm
	c ← a (10,0) - 322 nm	c → X (10,4) - 305 nm
	c ← a (5-10,0)	c → X (0,6) - 422 nm (1)
$c\ ^1\Sigma_u^-$	B ← c (0,0) - 599 nm	B → X (0,13) - 323 nm
	B ← c (1,0) - 575 nm	B → X (1,10) - 282 nm
	B ← c (2,0) - 554 nm	B → X (2,9) - 266 nm
$C\ ^3\Delta_u$	B ← C (0,0) - 665 nm	B → X (0,13) - 323 nm
	B ← C (1,0) - 636 nm	B → X (1,10) - 282 nm
	B ← C (2,0) - 610 nm	B → X (2,9) - 266 nm
	B ← C (3,0) - 587 nm	B → X (3,7) - 244 nm
	B ← C (4,0) - 566 nm	B → X (4,7) - 241 nm
$A\ ^3\Sigma_u^+$	B ← A (0,0) - 697 nm	B → X (0,13) - 323 nm
	B ← A (1,0) - 665 nm	B → X (1,10) - 282 nm
	B ← A (2,0) - 637 nm	B → X (2,9) - 266 nm
	B ← A (3,0) - 612 nm	B → X (3,7) - 244 nm
	B ← A (4,0) - 590 nm	B → X (4,7) - 241 nm
	B ← A (5,0) - 570 nm	B → X (5,6) - 229 nm

(1) Tests for vibrational quenching of the laser-excited species.
(2) Tests for quenching of the laser-excited species into the c $^1\Sigma_u^-$ state.

TABLE 5

TRANSITIONS USED IN LIF EXPERIMENTS ON VIBRATIONALLY EXCITED O_2 THAT USED LASER EXCITATION TO THE A AND B STATES

State to be Detected	Laser Excitation	Fluorescence
$X\ ^3\Sigma_g^-$ (v=3)	B ← X (0,3) - 223 nm	B → X (0,12) - 311 nm
	B ← X (0,3) - 223 nm	B → X (0,13) - 323 nm
$X\ ^3\Sigma_g^-$ (v=4)	B ← X (2,4) - 224 nm	B → X (2,8) - 257 nm
$X\ ^3\Sigma_g^-$ (v=5)	B ← X (5,5) - 222 nm	B → X (5,10) - 263 nm
$X\ ^3\Sigma_g^-$ (v=2)	A ← X (5,2) - 282 nm	A → X (5,7) - 355 nm
	A ← X (5,2) - 282 nm	A → X (0,8) - 431 nm (1)
	A ← X (5,2) - 282 nm	c → X (0,6) - 422 nm (2)
$X\ ^3\Sigma_g^-$ (v=3)	A ← X (5,3) - 295 nm	A → X (5,7) - 355 nm
	A ← X (5,3) - 295 nm	A → X (0,8) - 431 nm (1)
	A ← X (5,3) - 295 nm	c → X (0,6) - 422 nm (2)
$X\ ^3\Sigma_g^-$ (v=4)	A ← X (5,4) - 308 nm	A → X (5,7) - 355 nm
	A ← X (5,4) - 308 nm	A → X (0,8) - 431 nm (1)
	A ← X (5,4) - 308 nm	c → X (0,6) - 422 nm (2)

(1) Tests for vibrational quenching of the excited species.
(2) Tests for quenching of the excited species into the c $^1\Sigma_u^-$ state.

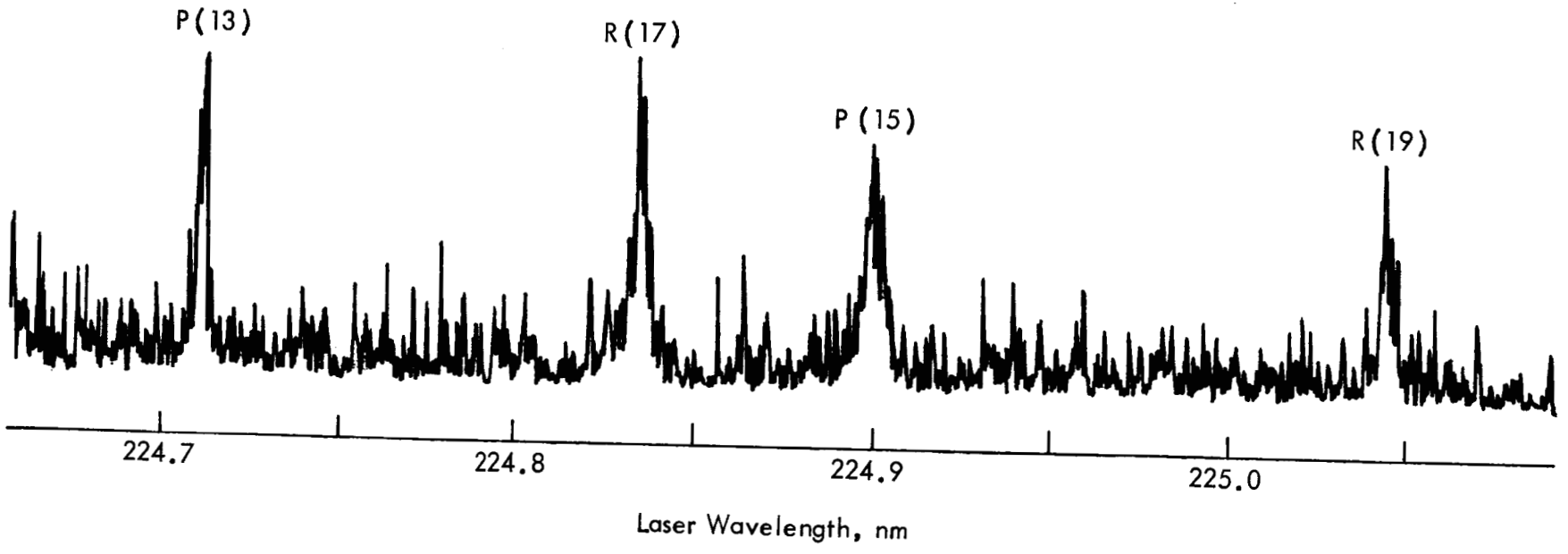

Figure 9 - LIF Spectrum of X $^3\Sigma_g^-$ (v=4) Level. Laser Excitation occurs on the rovibronic transitions of the B(v=2) ← X(v=4) band. Fluorescence is collected from the B(v=2) → X(v=8) band at 257 nm. The spectrum was taken in 100 torr of oxygen at 1500K.

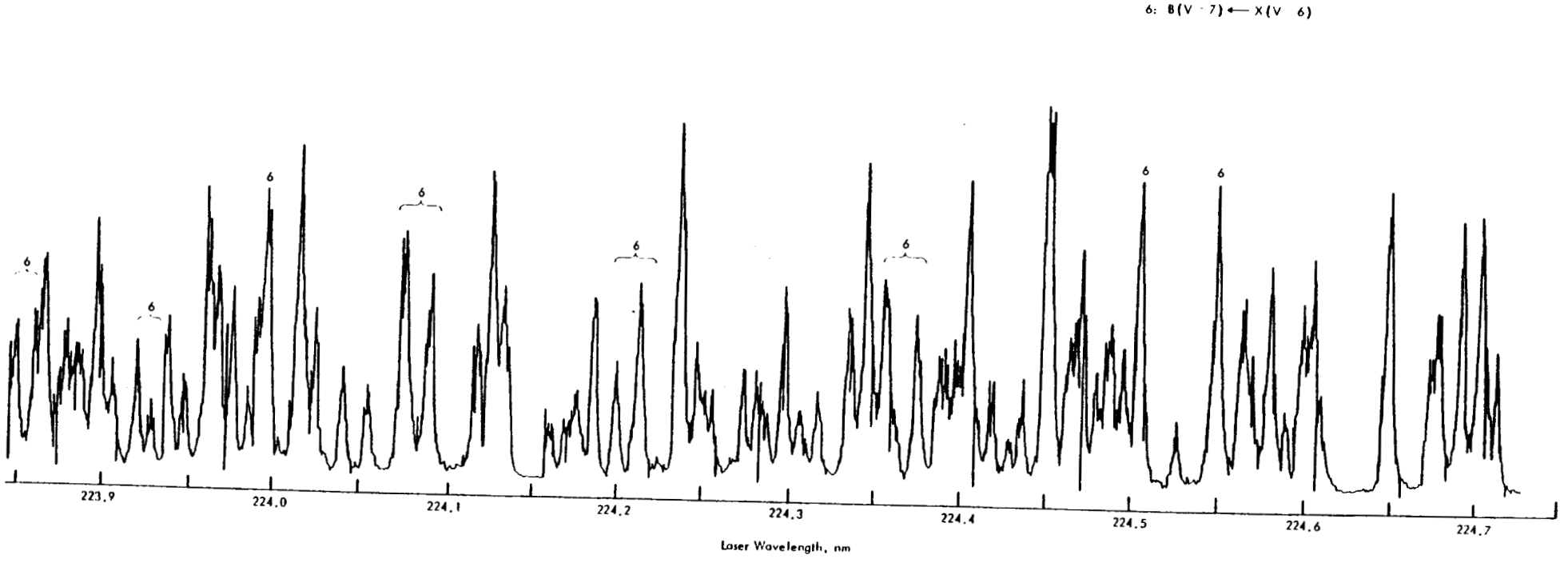

Figure 10 - LIF Spectrum of X $^3\Sigma_g^-$ (v=6). Laser excitation occured on the rovibronic transitions of the B(v=7) ← X(v=6) band. Fluorescence was collected from the B(v=7) → X(v=10) band at 255 nm. The spectrum was obtained in the hot gas flow from the RF discharge flow reactor.

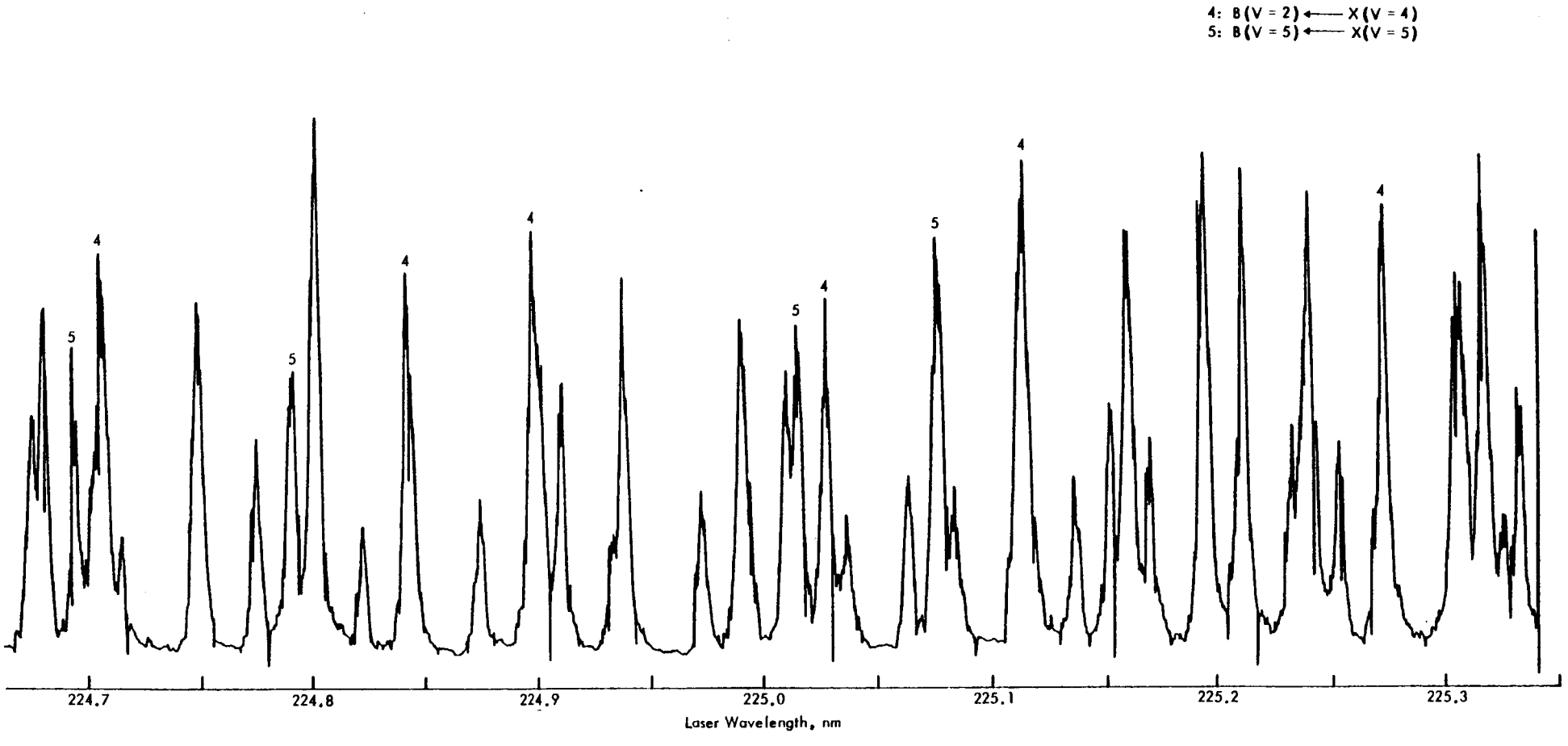

Figure 11 - LIF Spectrum of X $^3\Sigma_g^-$ (v=4,5). Laser excitation occurred on the rovibronic transitions of the B(v=2) ← X(v=4) band with fluorescence collected from the B(v=2) → X(v=8) band at 257 nm and of the B(v=5) ← X(v=5) band with fluorescence collected from the B(v=5) → X(v=9) band at 254 nm. The spectrum was obtained in the hot gas flow from the RF discharge flow reactor.

Table 6 presents the relative populations calculated for the v=3,4,5 vibrational levels of the ground electronic state of oxygen at various temperatures. At most, 3.1% of the molecules in the v=4 or v=5 vibrational levels of O_2 are in one of the rovibronic states excited by the laser. Since the concentration of v=5 molecules was just sufficient for detection at 1500K and an oxygen pressure equal to 100 torr, we obtained a minimum detectable concentration for specific rovibronic states of O_2 equal to 1.1×10^{13} cm^{-3} by LIF from the B-state. This is about 5,500 times larger than the detectivity for NO molecules.

TABLE 6

RELATIVE VIBRATIONAL LEVEL POPULATIONS OF THE OXYGEN X STATE VERSUS TEMPERATURE

	300K	1500K	3000K
v = 1	0.000572	0.174	0.247
v = 2	3.6E-07	0.0400	0.118
v = 3	2.6E-10	0.00939	0.0574
v = 4	2.1E-13	0.00226	0.0281
v = 5	1.9E-16	0.000555	0.0139
v = 6	1.7E-20	0.000139	0.00699
v = 7	1.9E-23	0.000036	0.00354
v = 8	2.4E-26	9.3E-06	0.00181
v = 9	3.3E-29	2.5E-06	0.000939
v = 10	5.2E-32	7.0E-07	0.000492

In contrast to LIF detection of NO molecules, LIF detection of O_2 is dominated by nonradiative loss of the laser-excited state. Equation 5 may then be written:

$$I = n\ f\ V\ e\ A/(A + Q_{nr}) \qquad (6)$$

where A is the reciprocal of the radiative lifetime for the laser-excited state and Q_{nr} is the rate of excited state loss by nonradiative processes.

Nonradiative loss of the O_2 B-state occurs because this state is predissociated. That is, B-state molecules dissociate within a few picoseconds after they are formed because the B-state potential energy curve crosses repulsive potential energy curves arising from ground state O-atoms (cf. Figure 1). The laser intensity was sufficient to saturate the B (v=5) ← X (v=5) transition. Since the B-state predissociates in a time much less than the laser pulse duration, virtually all of the lower state O_2 molecules were pumped to the upper state. The appropriate value for f is therefore 1.0 (compared with f = 1/2 for NO). It follows that the value of Q_{nr}/A in Equation 4 is about 11,000. This result is consistent with the known values of the lifetimes, i.e., a few picoseconds for predissociation and a few tens of nanoseconds for radiation.

The minimum detectable concentration of a specific rovibronic state of O_2, via LIF from the O_2 B-state is thus, in these experiments, about 10^{13} cm^{-3}. This explains why electronically exicted O_2 molecules were not detected in the products of atom recombination. The O-atom concentration was at most 10^{15} cm^{-3}. Not all of the atoms recombine and the recombination products will be distributed among several electronic and vibrational states of O_2. Also, a maximum of about 3% of the molecules in any specific vibrational state are in a given rovibronic state excited by the laser. Thus, the concentration of excited molecules produced by atom recombination could not be sufficient for detection.

Inadequate sensitivity for LIF detection of O_2 via excitation to the O_2, c, C, and A states is also attributed to nonradiative loss of the laser excited molecules and also to values of f much less than unity due to small absorption coefficients for transitions to these states. The most favorable case would seem to be for laser excitation to the A-state and LIF detection of A → X emission. In this case, the value of A in Equation 4 is about 6 s^{-1} and the value of Q_{nr} is given by:

$$Q_{nr} = \Sigma\, k_{q,i}\, n_i \qquad (7)$$

where $k_{q,i}$ and n_i are the collisional quenching rate constants and concentrations for the various species that quench emission from the O_2 A-state. Values of $k_{q,i}$ reported by Kenner and Ogryzlo[17,18] and Slanger et al.,[16] are given in Table 7. These rate constants are large enough to account for the absence of detectable LIF from A-state molecules in our experiments. Since the quenching rate is proportional to the O-atom or O_2-molecule concentration, as is the number of laser excited species, the LIF intensity will depend on concentration only when quenching is not the dominant A-state loss process. Therefore, experiments at higher pressures would not improve the sensitivity of this method for LIF detection of O_2 molecules.

B. Field Ionization Experiments

Preliminary testing of the field ionization apparatus was carried out by operating the tip at a fixed voltage and turning the microwave discharge on and off. The following typical values for the field ion current, j, were obtained at an applied voltage of 2,700 v:

Atoms off: $j = 1.35 \times 10^{-11}$ amp

Atoms on: $j = 1.60 \times 10^{-11}$ amp

This result indicated that the field ionization current may be responding to the presence of atoms and excited molecules in the flow from the discharge. However, subsequent experiments with variable and larger values for the applied voltage gave more complex behavior.

When the discharge was turned on, a large current was measured at zero voltage applied to the field ionization apparatus. This current was apparently due to collection of electrons in the flow from the discharge. It decreased to zero as the voltage was increased, after which an increase due to field ionization of neutral molecules could be observed. Figure 12 presents plots of the current-voltage curves with the discharge on and off in the region of higher applied voltages at which field ionization occurred. Insertion of a nickel coil into the flow from the discharge produced a result essentially the same as when the discharge was off.

TABLE 7

RATE CONSTANTS FOR QUENCHING OF FLUORESCENCE FROM O_2 A $^3\Sigma_u^+$ AND c $^1\Sigma_u^-$

Quenched State	Quenching Species	Quenching Rate Constant ($cm^3\ s^{-1}$)	Reference
c (v = 0)	O_2	3×10^{-14}	16
	$O_2(a\ ^1\Delta_g)$	6.0×10^{-12}	16
	$O(^3P)$	5.9×10^{-12}	16
	Ar	6×10^{-16}	16
A	O_2	2.9×10^{-13}	17
	$O(^3P)$	0.9×10^{-11}	17
	Ar	8.6×10^{-16}	17
A (v=2)	O_2	1.3×10^{-13}	16
	$O_2(a\ ^1\Delta_g)$	8.1×10^{-11}	16
	$O(^3P)$	1.3×10^{-11}	16
	Ar	7.2×10^{-16}	16
A (v=8)	O_2	$> 8 \times 10^{-11}$	15

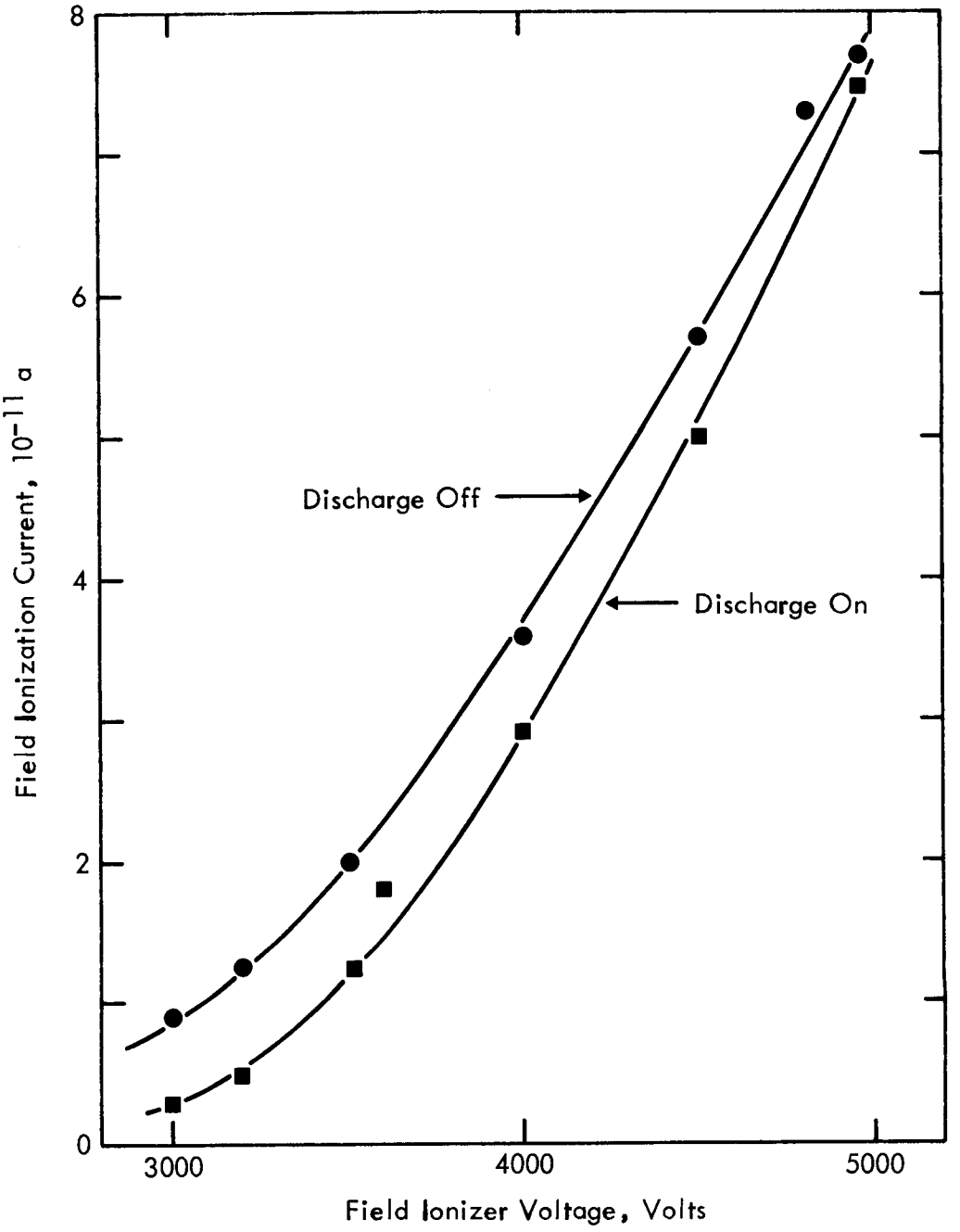

Figure 12 - Field Ionization Currents in Oxygen and Partially Dissociated Oxygen at High Values of the Applied Voltage

C. Molecular Beam Mass Spectrometric Experiments

Figure 13 shows the variation of O^+ ion intensity with RSI specimen position relative to an axis through the MBMS orifice for experiments carried out at a pressure of 133 Pa (1.0 torr) and for specimen temperatures of 300 and 900K ± 50K. The MBMS orifice location was determined to ± 1 mm in these experiments but remained constant to about ± 0.1 mm between experiments. The value measured for the O^+ ion intensity when the RSI specimen blocked direct flow from the discharge tube to the MBMS orifice equaled that obtained from dissociative ionization of O_2 when the discharge was turned off.

Figures 14 to 16 present the variations of O^+, O_2^+, and O_3^+ ion intensities with RSI specimen position for experiments at a pressure of 400 Pa (3.0 torr) and RSI specimen temperatures equal to 300 ± 50K. These data were measured relative to the Ar ion intensity, which served as an internal standard to account for small variations in MBMS sensitivity with gas temperature as the RSI position was changed. The O^+ intensities were corrected for dissociative ionization of O_2 molecules. Figure 17 presents the variation of O^+ ion intensity with the position of a nickel specimen of identical shape to the RSI specimen.

The intensities of O^+, O_2^+, and O_3^+ (relative to the Ar^+ intensity) are summarized in Table 8 for RSI and nickel specimens. The atomic oxygen concentration in the flow from the discharge can be calculated from these data in two ways. First, the 17% increase in O_2 signal upon loss of the O-atoms as the sample is inserted indicates that the initial O-atom concentration was 34% of the O_2 concentration. The second method for calculating O-atom concentrations is to use the measured $O:O_2$ intensity ratio.

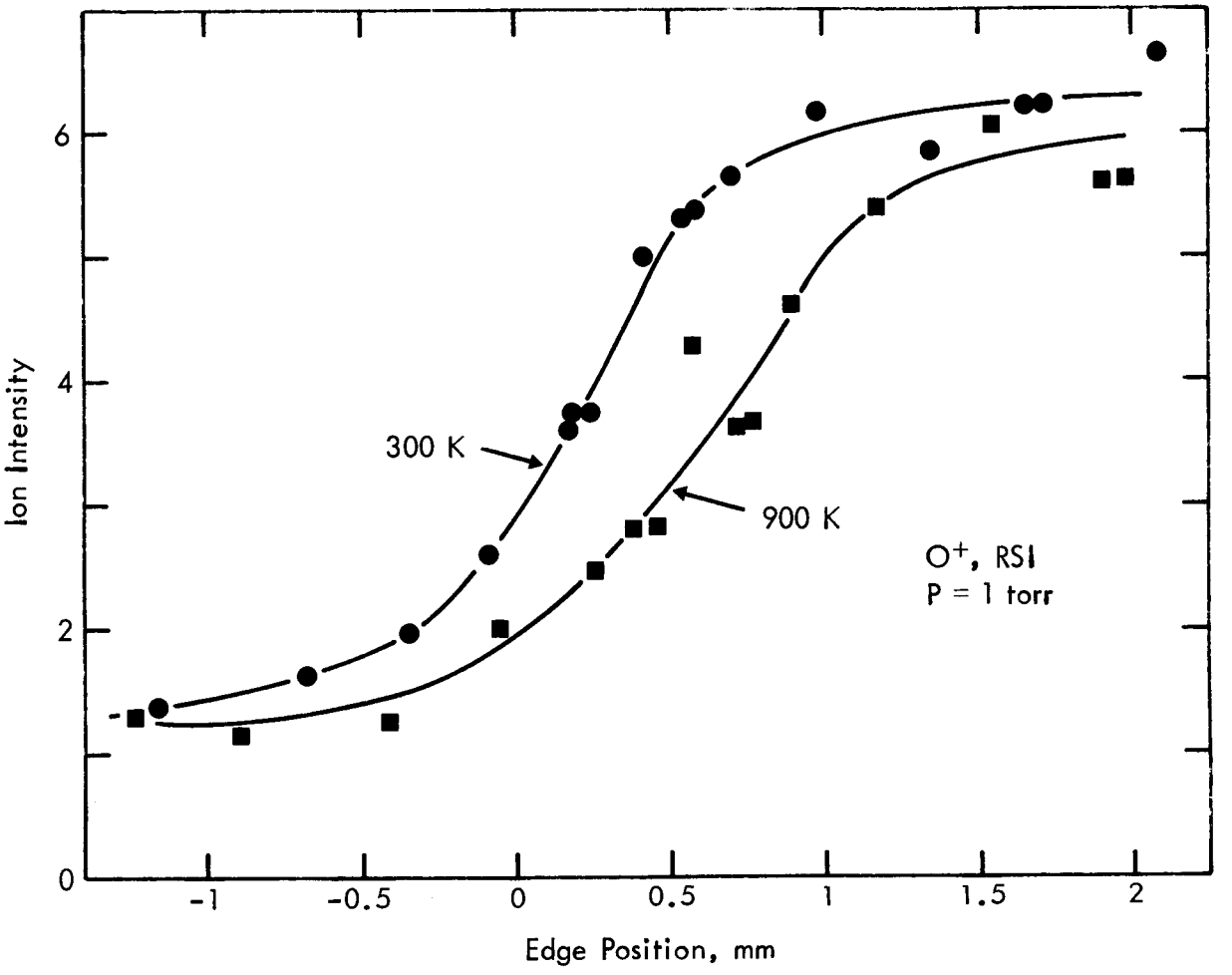

Figure 13 - Oxygen Atom Ion Intensity Versus RSI Specimen Position in MBMS Experiment at P = 130 Pa (1 torr)

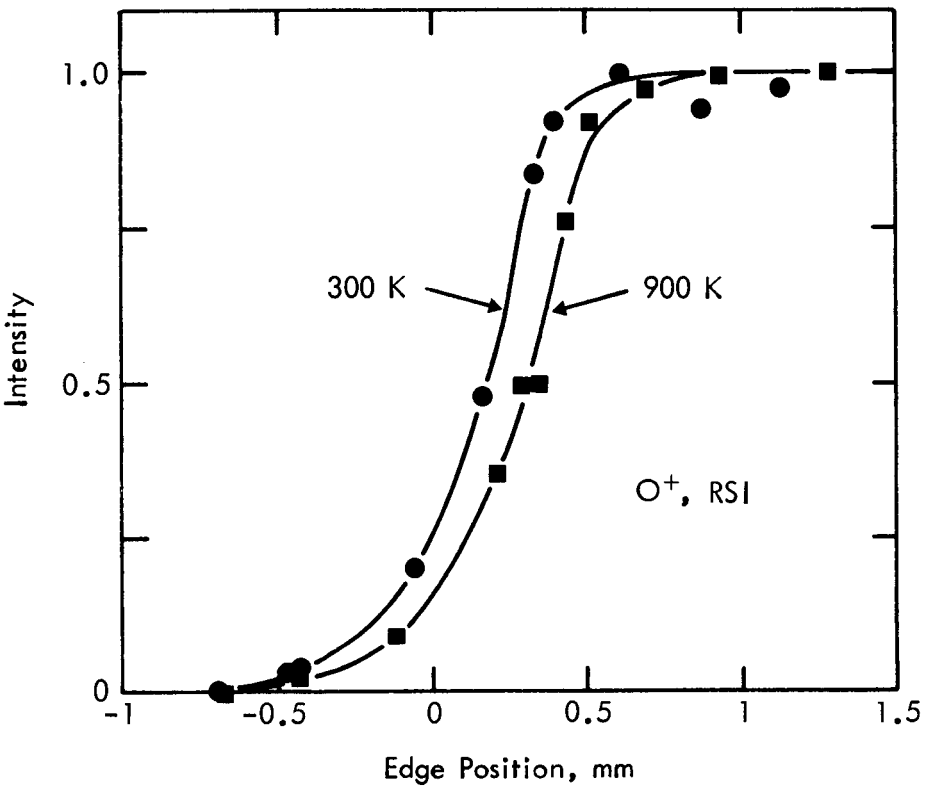

Figure 14 - Oxygen Atom Ion Intensity Versus RSI Specimen Position in MBMS Experiment at P = 400 Pa (3 torr)

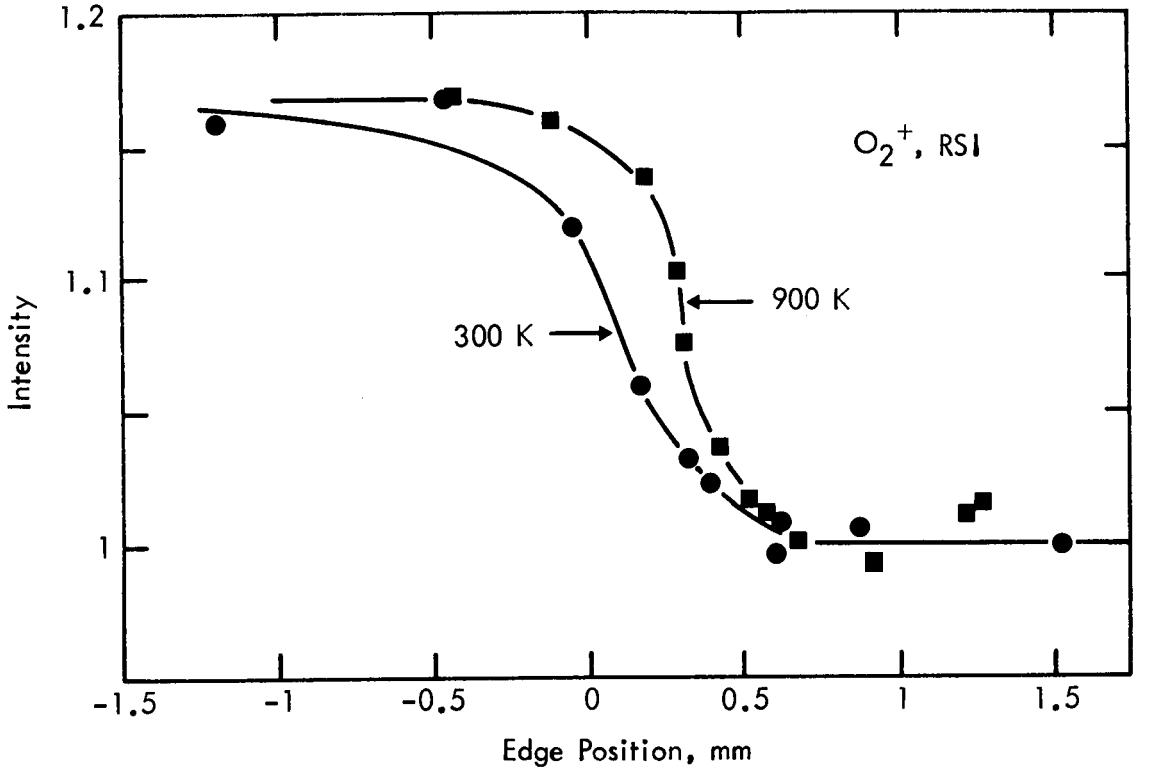

Figure 15 - Oxygen Molecular Ion Intensity Versus RSI Specimen Position in MBMS Experiment at P = 400 Pa (3 torr)

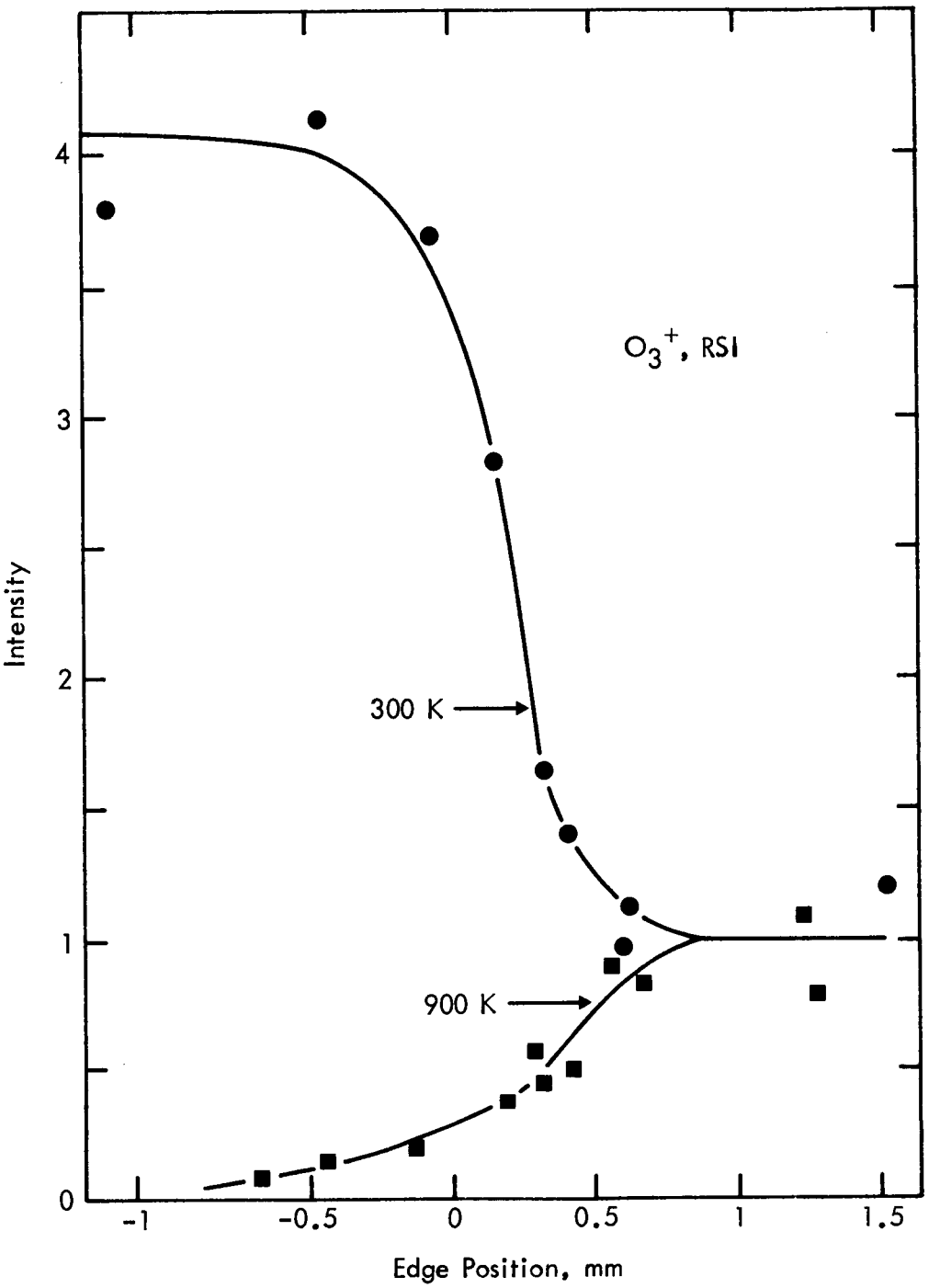

Figure 16 - Ozone Ion Intensity Versus RSI Specimen Position in MBMS Experiment at P = 400 Pa (3 torr)

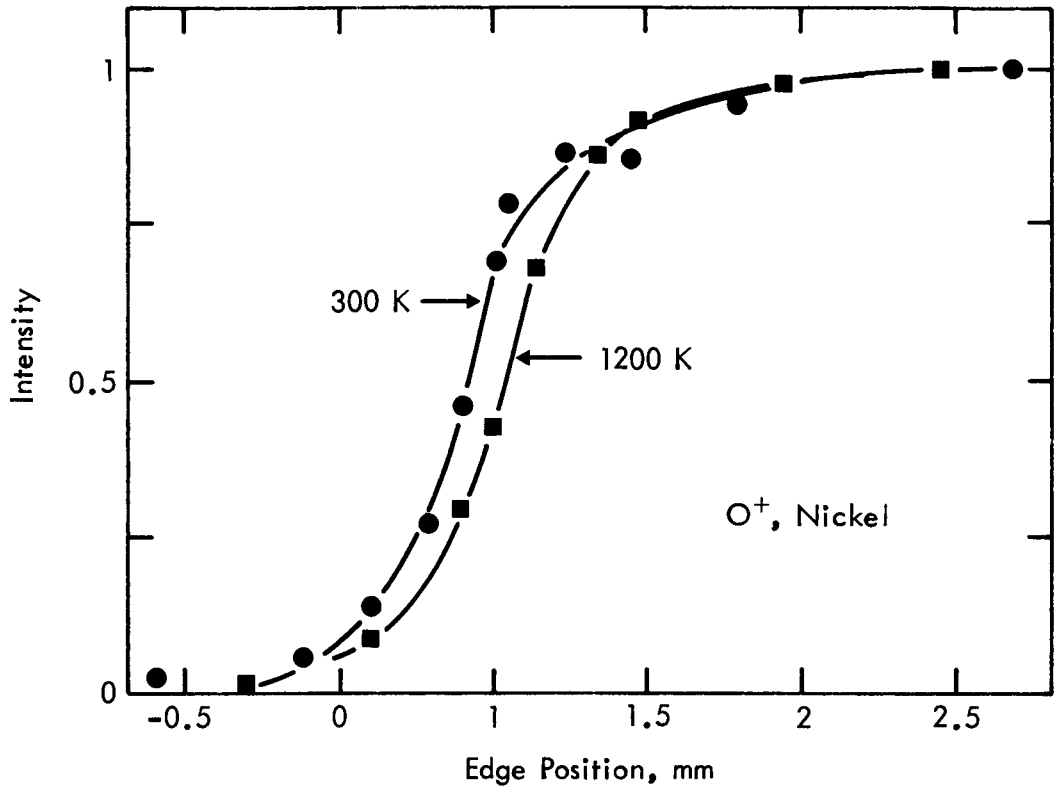

Figure 17 - Oxygen Atom Ion Intensity Versus Nickel Specimen Position in MBMS Experiment at P = 400 Pa (3 torr)

This ratio was corrected for experimental ionization cross sections[19] and measured mass filter transmissions and multiplier efficiencies. A correction for mass discrimination in the molecular beam was also required. This was made assuming a fully developed free-jet expansion and using the mass separation correction given by Greene et al.[20] The oxygen atom concentration obtained by this procedure was 0.29 of the O_2 concentration, in good agreement with that obtained by the first method.

TABLE 8

RELATIVE INTENSITIES FOR OXYGEN SPECIES

Species	O_2	O	O_3
Sample withdrawn	1.000	0.120	2.2×10^{-4}
Sample inserted:			
RSI, 300K	1.17	0.00	8.9×10^{-4}
Nickel, 300K	1.17	0.00	2.8×10^{-4}
RSI, 900K	1.17	0.00	0.00
Nickel, 1200K	1.17	0.00	0.00

The concentration of ozone was calculated from the O_3^+ intensity relative to O_2^+ using the second method described above. The correction for the fragmentation of O_3 was made using the data of Anderson and Mauersberger.[21] The resulting ozone concentrations, together with the oxygen atom concentrations are summarized in Table 9. It can be seen that the concentration of ozone was found to be very small. This does not directly demonstrate (as discussed later) that ozone production contributes negligibly to the mass and energy balances for O-atom loss on RSI and nickel.

TABLE 9

RELATIVE CONCENTRATIONS OF OXYGEN SPECIES

Species	O_2	O	O_3
Sample withdrawn	1.000	0.29	1.9×10^{-4}
Sample inserted:			
RSI, 300K	1.17	0	7.4×10^{-4}
Nickel, 300K	1.17	0	2.4×10^{-4}
RSI, 900K	1.17	0	0
Nickel, 1200K	1.17	0	0

V. DISCUSSION AND CONCLUSIONS

A. LIF Experiments

When considering the inability to detect electronically excited O_2 via LIF, there are several factors that are important. Most of the electronic transitions among the low lying states are forbidden by symmetry considerations. Furthermore, as shown in Figure 1, there is a shift of 0.3 to 0.4 angstrom in the internuclear distance at the bottom of the potential wells between the low lying X, a, and b states (below 2 ev) and the higher lying c, C, A, and B states (at 4 to 6.2 ev). Many of the electronic transitions of interest for laser excitation and for fluorescence involved one level in the lower group and one level in the higher group. The shift in the potential wells results in low values for the Franck-Condon factors. This, coupled with the symmetry problems, leads to very small transition strengths. Also, quenching becomes an important nonradiative loss process.

The laser intensity was not sufficient to excite a large fraction of the available species for many of the transitions that were investigated. It is clear, in fact, that detection of vibrationally excited O_2 would not be possible by LIF from the A-state even if the A $\leftarrow$ X transition could be

saturated. Consider, for example, excitation to A(v=2) for which the rate constant for O_2 quenching is relatively small. The A-factor for this state is about 6 s^{-1}. It follows that the minimum detectable signal, 5 photons per laser pulse, would be achieved only if the population of the particular rovibronic state to be detected exceeds about 4×10^{-5} of the total O_2 concentration. With, say, 0.03 of the molecules in a given vibrational level that are in a given rotational state, we need at least 10^{-3} of the molecules in the vibrational state of interest. Table 6 shows that this possibility does not significantly enhance the demonstrated ability to detect vibrationally excited O_2 via LIF from the B-state.

The minimum concentration of O_2 molecules that can be detected by LIF was therefore quite large. Much better sensitivity was achieved for NO molecules, and would also be possible via 2-laser LIF techniques for N_2 molecules.[7]

The high quenching rates that have been demonstrated for the O_2 A and c states (c.f. Table 7) mean that molecules that may be produced in these states by heterogeneous recombination on space vehicle TPS materials would be quenched after only a few collisions with other gas phase molecules. Consider, for example, the fate of A-state molecules in a space vehicle reentry environment in which oxygen is fully dissociated at a stagnation point air pressure of 30 torr and at a space vehicle surface temperature of 1500K. The O-atom concentration would then be ca. 6.4×10^{16} cm^{-3} (assuming N_2 is not dissociated), and the quenching rate of the O_2 A-state molecules by O-atoms would be about 6×10^5 s^{-1}. The A-state molecules would then be quenched within a distance less than 0.01 cm from the surface on which they were formed. This is not to say that the energy of these molecules would be released by quenching, for the quenched products may also be excited molecules, e.g., vibrationally excited ground state molecules.

B. Field Ionization Experiments

It was apparent from the field ionization experiments that electrons from the discharge were collected by the field ionization apparatus at lower values of the applied voltage. At high fields, the negative potential on the ring electrode of the field ionizer suppresses flow of electrons to the field ionization tip and current collecting leads, which were at ground potential in the apparatus.

The currents measured at high values of the applied voltage were larger with the discharge off than with it on, and also increased when the atom flow from the discharge was removed by inserting a nickel catalyst coil into the flow. These results indicate that oxygen atoms were the predominant new species delivered to the field ionization tip when the discharge was turned on. The ionization energies of relevant species are:

Ground state O_2 ($^3\Sigma^+$):	12.98 ev
Singlet delta O_2 ($^1\Delta g$):	11 ev
Ground state O-atoms (3P)	13.6 ev

Thus the effect of partial dissociation of O_2 in the discharge was to reduce the field ion currents because the ionization energy of the added atomic oxygen is greater than that of the O_2 molecules that were removed.

C. MBMS Experiments

Only small fractions of the O-atoms that are lost at nickel and RSI catalyst surfaces appear as O_3 in the gas sampled by the MBMS orifice. This does not provide conclusive proof that ozone is a negligible direct product of heterogeneous O-atom reaction, as will be discussed below. In any case, MBMS observation of ozone formation on catalysts has been demonstrated for the first time. Ozone is an easily observed species for which more detailed MBMS investigations of its heterogeneous reactions are possible. A deeper understanding of the kinetics and mechanisms of O-atom reactions at surfaces may thus be obtained.

It is evident that the surface-catalyzed reaction rates were controlled by the rate of O-atom diffusion to the catalyst. In all cases, the measured concentration of O-atoms was reduced to less than half its value in the flow from the discharge before the catalyst material intercepted the flow sampled by the MBMS orifice. The O-atom concentration just at the catalyst surface would be even smaller because the measured concentration reflects mixing with higher concentration gas in the distance between the catalyst and MBMS orifice.

The product distributions that were observed may not be primary product distributions for O-atom loss. Suppose, for example, that ozone is formed by surface catalyzed $O + O_2$ reaction and lost by surface catalyzed $O + O_3$ reaction. The measured product distribution would then depend on the rates of ozone diffusion into the ambient gas and of ozone loss by the heterogeneous reaction. A fast ozone loss reaction could thus have given the high temperature results even if ozone was a major primary product of O-atom loss. That is, when both ozone formation and destruction are fast, local thermodynamic equilibrium (i.e., no ozone) will be achieved at the catalyst surface. Therefore, the results do not eliminate ozone formation as a significant contributor to the small energy accommodation coefficients for O-atom loss that have been measured on nickel[13] and inferred for RSI.

Calculations of atom loss probabilities from the MBMS results were not attempted because (1) an accurate model of mass transport and mixing in the experiments was not available and (2) the O-atom concentrations that were measured were evidently more sensitive to diffusion than heterogeneous reaction rates.

Improved sensitivity to the intrinsic product distribution would best be obtained if the MBMS orifice sampled gas at the catalyst surface. This could be done by forming the MBMS orifice from the catalyst of interest as illustrated in Figure 18. The technique has been successfully used by Greene et al.,[22,23] for other types of experiments but was not attempted here due to the estimated cost and time required to relocate laser and/or

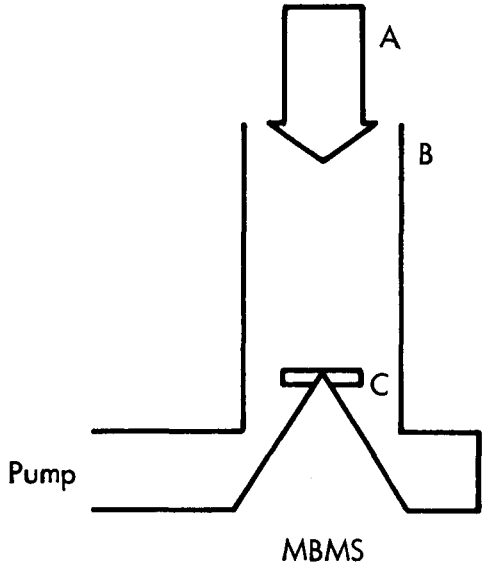

SIDE VIEW

Figure 18 - Schematic Diagram of Method for MBMS Measurement of Intrinsic Product Distributions and Kinetics for Surface Catalyzed Reactions in Dissociated Air. A - CW CO_2 laser beam and co-axial dissociated gas flow; B - vacuum wall of apparatus; C - catalyst material mounted on MBMS sampling orifice.

MBMS equipment. The catalyst would be attached to the MBMS orifice and heated by a CW CO_2 laser beam that is co-axial with the dissociated gas flow. Diffusion limitations on the O-atom concentration at the catalyst surface would still occur unless the pressure was quite small. However, O, O_2, and O_3 concentrations would be measured just at the surface to obtain intrinsic product distributions.

MBMS study of surface catalyzed O_3 formation from O + O_2 mixtures could be easily extended to the study of N_2O formation in partially dissociated air. It would also be helpful to incorporate arc jet or other discharge equipment for better simulation of space vehicle re-entry environments than was achieved with the microwave and inductively coupled RF discharge flow reactors used in this work. The influence of surface-catalyzed formation of ozone and nitrous oxide on the heating rates for TPS materials during space vehicle entry of the atmosphere may thus be established.

VI. RECOMMENDATIONS FOR FUTURE WORK

A major emphasis in these studies was on experiments utilizing laser-induced fluorescence. Although some useful data were obtained, the sensitivity with which excited oxygen molecules could be detected by LIF proved to be too small under conditions for which the kinetics of heterogeneous O-atom reactions could be studied. An alternative technique, molecular beam mass spectrometry (MBMS), was shown in limited experiments to be readily adaptable to the measurement of the O-atom loss and determination of species produced by atom recombination. The use of MBMS in the experimental configuration shown in Figure 18 should provide definitive data on atom recombination and other phenomena which take place at the gas-surface interface under space vehicle re-entry conditions. In addition, this experiment should be susceptible to theoretical analysis; and would allow values for the atom recombination coefficient, γ, to be derived from the results.

It is therefore recommended that a more extensive series of MBMS experiments, using the "surface-sampling" technique of Figure 18, be carried out to elucidate atom recombination and other phenomena which occur at relevant surfaces under re-entry conditions. Such studies should be extended to include all species, since N_2O or other molecules or free radicals could be important in energy transfer. In addition to these "chemical" data and accommodation coefficients, appearance potential measurements could be utilized to definitively detect the presence of any significant concentration of excited species. The results of continued experiments should thus provide hitherto unavailable information about re-entry processes.

VII. REFERENCES

1. Breen, J., R. Cibrian, W. N. Delgass, N. G. Krishnan, P. C. Nordine, and D. E. Rosner, "Catalysis Study for Space Shuttle Vehicle Thermal Protection System," Final Report to NASA-Johnson Space Center, Houston, TX, Yale University (1973); NASA CR-134124, October 1973.

2. Scott, C. D., "Catalytic Recombination of Nitrogen and Oxygen on High-Temperature Reusable Surface Insulation," in Aerothermodynamics and Planetary Engry, A. L. Crosbie, ed., Vol. 77 of Progress in Astronautics and Aeronautics, pp. 192-212 (1981).

3. Vought Missiles and Space Company Reports T143-5R-00044 (1971) and T143-5R-00124 (1972).

4. Scott, C. D., "Effects of Nonequilibrium and Wall Catalysis on Shuttle Heat Transfer," J. Spacecraft and Rockets, 22, 489 (1985).

5. Stewart, D. A., J. V. Rakich, and M. J. Lanfranco, "Catalytic Surface Effects Experiment on the Space Shuttle," Progress in Astronautics and Aeronautics: Thermophysics of Atmospheric Entry, Vol. 82, T. E. Horton, ed., AIAA, New York, 1982, pp. 248-272.

6. Rakich, J. V., D. A. Stewart, and M. J. Lanfranco, "Results of a Flight Environment on the Catalytic Efficiency of the Space Shuttle Heat Shield," AIAA Paper 82-0944, June 1982.

7. Nordine, P. C., "Literature Survey: The Study of Excited Oxygen Molecule Gas Species Production and Quenching on Thermal Protection System Materials," Midwest Research Institute, Kansas City, MO, March 1985.

8. Krupenie, P. H., "The Spectrum of Molecular Oxygen," J. Phys. Chem. Ref. Data, 1, 423 (1972).

9. Saxon, R. P., and B. Liu, "Ab Initio Configuration Interaction Study of the Valence States of O_2," J. Chem. Phys., 67, 4779 (1978).

10. Slanger, T. G., J. Chem. Phys., 69, 4779 (1978).

11. Golde, M. F., and B. A. Thrush, Rep. Prog. Phys., 36, 1285 (1973).

12. Ogryzlo, E. A., "The Nature of Singlet Oxygen," in Singlet Oxygen, R. Ranby and J. F. Rabek, eds., Wiley Interscience, NY, pp. 4-11 (1976); E. A. Ogryzlo, "Physical Quenching of Singlet Oxygen, ibid, pp. 17-26.

13. Melin, G. A., and R. J. Madix, "Energy Accommodation During Oxygen Atom Recombination on Metal Surfaces," Trans. Farady Soc., 67, 198 (1971).

14. Manilla, G., and P. Harteck, J. Chem. Phys, 34, 2177 (1961); Harteck, P., and R. R. Reeves, Jr., Discuss. Farady Soc., 37, 82 (1964).

15. Lee, M. P., P. H. Paul, and R. K. Hanson, "Laser-Fluorescence Imaging of O_2 in Combustion Flows Using an ArF Laser," Opt. Lett. 11, 7-9 (1986).

16. Slanger, T. G., W. K. Bischel, and M. J. Dyer, "Photoexcitation of O_2 at 249.3 nm," Chem. Phys. Lett., 108, 472-474 (1984).

17. Kenner, R. D. and E. A. Ogryzlo, Can. J. Chem., 61, 921-926 (1983).

18. Kenner, R. D. and E. A. Ogryzlo, Intern. J. Chem. Kinetics, 12, 501-508 (1980).

19. Pottie, R. F., J. Chem. Phys., 44, 916 (1966).

20. Greene, F. T., J. Brewer, and T. A. Milne, J. Chem. Phys., 40, 1488 (1964).

21. Anderson, S., and K. Mauersberger, Rev. Sci. Instrum., 52, 1025 (1981).

22. Greene, F. T., G. Radolovich, and P. W. Dimiduk, "An Experimental Investigation of Mechanisms of Laser Degradation of Materials," Proceedings, 2nd DOD Conference on Laser Effects/Hardening, NASA-Ames Research Center, Moffett Field, California (1975).

23. Isom, K. B., and F. T. Greene, "Studies of Nonequilibrium Combustion," Proceedings, 17th Joint Army-Navy-NASA-Air Force Combustion Meeting, Vol. IV (1980).

VIII. DISTRIBUTION

NASA Lyndon B. Johnson Space Center
Contract No. NAS9-17261
Houston, Texas 77058
Attn: Dr. Carl D. Scott/ED3 (25 copies)
Attn: Mr. Mark A. Lucas/BE2 (1 copy)
Attn: JSC Technical Library/JM2 (2 copies)
Attn: JSC Technology Officer/AL32 (1 copy)

Midwest Research Institute
Dr. Paul C. Nordine
Dr. Frank Greene
Dr. Gordon Fujimoto

Professor Bret L. Halpern
Department of Chemical Engineering
Box 2159 Yale Station
New Haven, CT 06520